SKI Report 96:14

SITE-94

Simple Evaluation of Groundwater Flow and Radionuclide Transport at Äspö

Björn Dverstorp
Joel Geier
Clifford Voss

December 1996

ISSN 1104-1374
ISRN SKI-R--96/14--SE

SKI
STATENS KÄRNKRAFTINSPEKTION
Swedish Nuclear Power Inspectorate

SKI Report 96:14

SITE-94

Simple Evaluation of Groundwater Flow and Radionuclide Transport at Äspö

Björn Dverstorp [1]
Joel Geier [2]
Clifford Voss [3]

[1] Swedish Nuclear Power Inspectorate, Stockholm, Sweden
[2] Clearwater Hardrock Consulting, Monmouth, Oregon, USA
[3] U.S. Geological Survey, Reston, Virginia, USA

December 1996

Project Number 94259, 96063, 96100, 96138 and 96120

NORSTEDTS TRYCKERI AB
Stockholm 1997

PREFACE

This report concerns a study which is part of the SKI performance assessment project SITE-94. SITE-94 is a performance assessment of a hypothetical repository at a real site. The main objective of the project is to determine how site specific data should be assimilated into the performance assessment process and to evaluate how uncertainties inherent in site characterization will influence performance assessment results. Other important elements of SITE-94 are the development of a practical and defensible methodology for defining, constructing and analyzing scenarios, the development of approaches for treatment of uncertainties and evaluation of canister integrity. Further, crucial components of an Quality Assurance program for Performance Assessments were developed and applied, including a technique for clear documentation of the Process System, the data and the models employed in the analyses, and of the flow of information between different analyses and models.

Björn Dverstorp
Project Manager

Abstract

A simple evaluation of groundwater flux and potential for radionuclide transport at the Äspö site, in southeastern Sweden, based on fundamental hydrologic principles, indicates that, based upon the data that are available from surface-based investigations (*i.e.*, geological, geophysical, and hydrological observations in boreholes and at the surface) it is not possible to confirm that the bedrock has a high capacity to retard radionuclide release to the surface environment. This result is primarily due to the high spatial variability of hydraulic conductivity, and high uncertainty regarding the relationships among hydrologic and transport parameters within conductive elements of the bedrock.

A comparison between Äspö and seven other study sites in Sweden indicates that it is difficult or impossible to discriminate among these sites in terms of the geologic barrier function, based upon the types of data that are available from present-day, surface-based methods of site characterization (including measurements in boreholes). The availability of more surface-based data at Äspö, generated by an extensive site-characterization program, does not lead to a narrower predicted range of groundwater throughflux than for the other sites where much less data are available.

The analysis gives predictions of the groundwater flux through, and radionuclide transport from a hypothetical repository located in the bedrock. Groundwater flux is evaluated by a one-dimensional application of Darcy's law to a set of simple, potential pathways for groundwater flow from the repository, which are chosen to yield an appraisal of the wide bounds of possible system behavior. The configurations of the pathways are specified based on simple assumptions of flow-field structure, and hydraulic driving forces are specified based upon consideration of regional and local topographic differences. The analysis of flux is extended to seven other study sites in Sweden, to illustrate how the approach can be used to compare among sites. Transport of radionuclides within the groundwater pathways for Äspö is analyzed by considering a range of simple models for the pore geometry within conductive features, to account for large uncertainty in the relationships among hydrologic and transport parameters. Results are expressed in terms of a parameter group that has been shown to control the geologic barrier function, *i.e.* the capacity of the bedrock to retard the release of radionuclides to the surface environment.

Comparisons with more detailed hydrological modelling of Äspö show that, although the detailed models yield a reduction in the uncertainty regarding the capacity of the bedrock to retard radionuclide release, this reduction of uncertainty is not sufficient to distinguish between good and poor performance of the geologic barrier at the site. Although it is not certain that more definite predictions of the performance of the geological barrier at the site are achievable, additional types of measurements beyond the types of information that were obtained from surface-based measurements at Äspö would likely be needed to obtain this.

Abstract (Swedish)

Bergets barriäregenskaper har analyserats med hjälp av enkla beräkningar av grundvattenflöde och radionuklidtransport baserade på grundläggande hydrogeologiska principer och data från SKBs markbaserade platsundersökningar vid Äspö i sydöstra Sverige (d.v.s. geologiska, geofysiska och hydrogeologiska mätningar på markytan och i djupa borrhål). Analysen visar att tillgängliga data inte är tillräckliga för att otvetydigt verifiera att berget har en god förmåga att reducera eventuellt utläckage av radionuklider till biosfären. Detta beror i första hand på en stor rumslig spridning (variabilitet) av bergets vattengenomsläpplighet (hydraulisk konduktivitet) och avsaknad av data avseende hydrogeologiska och transportparametrar i vattenförande sprickor och sprickzoner.

En jämförelse mellan Äspö och sju andra undersökningsplatser i svensk berggrund indikerar att det är svårt eller omöjligt att rangordna platserna med avseende på bergets barriäregenskaper, givet tillgängliga data från markbaserade platsundersökningsmetoder (inklusive borrhål). Tillgång till avsevärt mer data (från markbaserade undersökningar) från Äspö i förhållande till de andra undersökningsplatserna ledde inte till en minskning av den beräknade spridningen av grundvattenflöden.

I analysen för Äspö bestämdes grundvattenflödet genom ett tänkt djupförvar och transport av radionuklider från förvaret till biosfären. Grundvattenflödet beräknades i en dimension med hjälp av Darcys lag, för ett antal idealiserade flödes- och transportvägar mellan det tänkta förvaret och biosfären. Ambitionen var att välja transportvägar på ett sådant sätt att de tillsammans ger en god täckning av alla möjliga transportvägar i berget. För varje flödes- och transportväg specificerades hydrauliska drivkrafter med utgångspunkt från regionala och lokala topografiska höjdskillnader. Beräkningarna av grundvattenflöde gjordes även för sju andra undersökningsplatser i Sverige för att illustrera hur analysen kan användas för att jämföra olika platser. För Äspö analyserades transport av radionuklider utmed de valda transportvägarna med hjälp av en serie idealiserade geometriska modeller av porstrukturen i vattenledande sprickor och sprickzoner. På motsvarande sätt som för flödesberäkningarna valdes ett brett spektrum av idealiserade transportmodeller för att kunna utvärdera de stora osäkerheter som råder kring sambandet mellan sprickors flödes- och transportegenskaper. Beräkningsresultaten presenteras i form av en parametergrupp som har visat sig vara ett bra mått på bergets barriärfunktion, d.v.s. bergets förmåga att begränsa utsläpp av radionuklider från berget till biosfären.

Jämförelser med en mer detaljerad hydrogeologisk modellering av Äspö visar att de beräknade osäkerheterna kring bergets barriäregenskaper blir mindre med mer komplexa modeller som kan ta hänsyn till mer av de tillgängliga data, men de kvarstående osäkerheterna är alltför stora för att man otvetydigt ska kunna avgöra om bergets barriärfunktion är bra eller dålig. För att åstadkomma mer precisa förutsägelser av bergets barriärfunktion krävs sannolikt andra typer av data än de som är tillgängliga från de markbaserade undersökningarna vid Äspö. Det är dock fortfarande en öppen fråga om ytterligare data leder till minskade osäkerheter i förutsägelser om bergets barriärfunktion eftersom en stor del av osäkerheterna beror på den stora spridningen (variabiliteten) av flödes- och transportegenskaper i kristallint berg.

Contents

Contents, ctd.

1 Introduction

This is a scoping analysis of groundwater flux through, and radionuclide transport from a repository in the Swedish crystalline basement. This analysis is part of the SITE-94 project (SKI, 1996), which has been conducted by the Swedish Nuclear Power Inspectorate (SKI). SITE-94 is a site-specific performance assessment for a high-level nuclear waste repository, hypothetically located at the site of the Swedish Hard Rock Laboratory (HRL) on Äspö, in southeastern Sweden. The layout and design of the hypothetical repository is described by SKI (1996). Nuclear waste within the repository is considered to be encapsulated within metal canisters, each of which is emplaced in its own deposition hole in the bedrock, located in the floor of deposition tunnels at a depth of approximately 500 m below the ground surface.

The objectives of this analysis, in relation to SITE-94, were:

- To determine broad bounds on the physically plausible ranges of hydrologic and transport parameters for the SITE-94 performance assessment.
- To identify major sources of uncertainty in hydrologic and transport parameters that have a critical impact on repository performance.

The types of predictions that are needed for the performance assessment include:

- Near-field flow (*i.e.* the rate of groundwater flow through the immediate vicinity of a canister-deposition hole), which affects radionuclide release from the spent-fuel canisters.
- Far-field flow and transport properties (*i.e.* parameters that characterize groundwater flow and potential for radionuclide transport through the rock that lies between the vicinity of the canisters and the ground surface), which are needed to predict radionuclide transport in the event that a canister begins to leak.

The first part of this analysis is a simple, scoping evaluation of groundwater flux. Groundwater flux is perhaps the most important hydrologic parameter for determining

safety, as the inflow to a repository affects changes in the geochemical conditions in the near field, and thus may control degradation of engineered barriers (*e.g.* the canister, the bentonite that is placed around the canister within the deposition hole, and the backfill that is emplaced in the deposition tunnels), while the outflow determines transport of released radionuclides. This scoping evaluation of flux is based on a simple, one-dimensional application of Darcy's law, with simple assumptions of flow field structure.

The analysis of groundwater flux considers seven study sites, besides the Äspö site, that have been characterized using surface and borehole investigations by the Swedish Nuclear Fuel and Waste Management Co. (SKB). It is emphasized that neither Äspö nor any of the seven SKB study sites is presently a candidate for the siting of an actual, radioactive-waste repository. The analysis employs the interpretations that have been developed by SKB of structures and hydrologic parameters at the eight sites. In all cases, the analysis relies exclusively upon data that have been gathered from the surface or from surface-based investigations in boreholes, prior to any excavation of shafts or tunnels. The level of detail in the site characterization, and in this analysis, varies from site to site. The most thorough analysis of groundwater flux is for the Äspö site, which is of primary interest for SITE-94, and for which a relatively intensive characterization of the site has been performed. The analyses for the other SKB study sites should be viewed mainly as illustrative of how this analysis could be extended to other, typical hydrogeological situations that might be encountered in Sweden, in the eventual siting of a repository.

The second part of this analysis is a scoping evaluation of radionuclide transport for the Äspö site. Radionuclide transport in the far field depends strongly upon both the groundwater flux and upon the structure of the fracture-system pore space through which the radionuclides are transported by the groundwater. The scoping evaluation of radionuclide transport is based on the simple evaluation of groundwater flux plus a variety of simple, idealized models for pore geometry within the transport pathways. The idealized pore-geometry models are used to demonstrate the wide variety of relationships that might exist between groundwater flux and effective parameters for transport, due to a scarcity of field data that might provide empirical constraints on these relationships.

Thirdly, the results of this analysis are used to evaluate the **geologic-barrier function,** which

is here defined as the capacity of the bedrock/groundwater system (or **geosphere**) to prevent or retard release of radionuclides to the surface environment (or **biosphere**) in the event of radionuclide release from the **engineered barriers** (such as canisters, tunnel backfill, *etc.*) within the repository. Two different criteria are used to evaluate the performance of the geologic barrier, the first based simply upon groundwater flux, and the second upon a parameter that summarizes the potential for radionuclide retardation along a given transport pathway, as introduced in Section 2.3.

Lastly, a comparison is given between the results of this analysis and the predictions of other, more detailed hydrogeological models that were employed in SITE-94. The comparison shows the effectiveness of the simple evaluation for evaluating the major hydrogeological sources of uncertainty.

2 Methodology

This scoping evaluation of groundwater flux and transport is focused on prediction of a few characteristic parameters that, based upon a general understanding of the processes involved, and consequence calculations (*i.e.*, predictions of the radiation dose that is delivered to the biosphere, for a given set of assumptions) carried out within SITE-94, are expected to control radionuclide release from canisters and transport to the biosphere. The analysis is restricted to a consideration of groundwater flow and the barrier function of the far-field geology. No attempt has been made to take into account other factors such as the influence of chemical conditions on transport, or the effects of the engineered barriers on flow and transport. However, the consequences of the predicted parameter ranges are discussed in terms of the more comprehensive radionuclide transport calculations that have been performed within SITE-94 (SKI, 1996).

2.1 Types of data used

The scoping evaluation of groundwater flux is based on the following types of data:

- Potential head gradients (from local and regional topography).
- Location and orientation of major fracture zones (from SKB's geological structural models of the sites).
- Estimates of hydraulic conductivity for the rock mass.
- Estimates of transmissivity ranges for major fracture zones.

The estimates of hydraulic conductivity and transmissivity are drawn from SKB's prior interpretations of hydrological tests in boreholes. These tests consisted primarily of injection (packer) tests, and were interpreted mainly by steady-state methods using conventional assumptions of cylindrical (radial) flow.

The scoping evaluation of transport parameters is based on the same types of data, plus a variety of simplified models for pore structure (as defined in Section 2.4).

2.2 Groundwater flow model

The analysis of groundwater flux is based upon a one-dimensional, mathematical model, known as Darcy's law. Darcy's law is generally accepted as being descriptive of fluid flow through porous or fractured media, and provides a convenient framework for discussing groundwater flow in various systems. According to this model, the volumetric flow rate, per unit cross-sectional area, from a given point x_A to a second point x_B is:

$$q = K \frac{\Delta h}{L} \tag{1}$$

where K [m/s] is the effective hydraulic conductivity of the rock between x_A and x_B, Δh [m] is the decrease in hydraulic head from x_A to x_B, and L [m] is the distance from x_A to x_B. The quantity q [m/s] is referred to as Darcy velocity or Darcy flux. Although q has the dimensions of velocity, it is not a true velocity, but rather a flux per unit area (flux density); hence the term Darcy flux might be preferred as more accurate. However, the term Darcy velocity, which is commonly used in the hydrology literature, is used here for consistency with the remainder of SITE-94.

For a conductive structure such as an individual fracture or a fracture zone, Darcy's Law is more naturally expressed in terms of the groundwater flux per unit width of the structure:

$$Q = T \frac{\Delta h}{L} \tag{2}$$

where T [m^2/s] is the coefficient of transmissivity for the structure, equal to the product K b where b [m] is the effective thickness of the structure and K is the effective hydraulic conductivity of the structure. The quantity Q [m^2/s] is related to the Darcy velocity within the structure as $q = Q/b$.

The Darcy velocity can be used as a preliminary indicator of geosphere performance, in terms of the geologic-barrier function. High Darcy velocities imply relatively poor performance of the geologic barrier, due to a greater potential for exposure of waste canisters

to changing geochemical conditions, and due to a potential for relatively rapid transport of radionuclides from failed canisters to the biosphere. However, it should be noted that the performance of the repository in terms of radionuclide transport depends strongly on parameters other than Darcy velocity, such as the discharge-path length, wetted surface area, and the geochemical properties of the rock and water. In SITE-94, efforts have been made to evaluate all meaningful combinations of Darcy velocity ranges with other important parameters (SKI, 1996).

2.3 Transport model

2.3.1 Processes influencing radionuclide transport

The transport of radionuclides in the far-field is affected by processes including the following:

- Advection
- Dispersion
- Surface sorption
- Matrix diffusion
- Radioactive decay

Other processes such as chemical reactions, precipitation/dissolution, and colloid-borne transport may also affect net radionuclide transport. However, these other processes are not considered in this simple evaluation. Within SITE-94 these processes were evaluated by scenario studies and/or qualitative assessments, rather than by quantitative calculations for the reference case, in part because the model that was used for far-field consequence calculations, CRYSTAL (Worgan and Robinson, 1995), does not account for these processes.

Advection is the motion of dissolved radionuclide species which is due to the net velocity $u = q/\theta$ of the water through the pore space, where θ is the effective porosity (defined as the ratio of the pore volume V_p encountered by the radionuclides to the "bulk volume," V_b, by which is meant the total volume of rock and pore space within which the transport pathway is contained). This velocity is therefore referred to as the advective velocity. In the absence of processes such as sorption and matrix diffusion, the median velocity of a concentration front through the rock is equal to the advective velocity.

Dispersion describes the spreading of a concentration front with transport distance. The causes of this spreading include both molecular diffusion, due to concentration gradients, and mechanical mixing effects, due to small-scale velocity variations (*e.g.* effects of surface roughness within fractures) and network effects (interconnections among distinct transport paths). The combined effects of advection and dispersion are described, for the case of 1-D

transport, by the advection-dispersion equation:

$$\frac{\partial C}{\partial t} = D_L \frac{\partial^2 C}{\partial x^2} - u \frac{\partial C}{\partial x} \qquad (3)$$

where $C(x,t)$ [mol/m^3] is the concentration as a function of transport distance x [m] and time t [s], and D_L [m^2/s] is the coefficient of longitudinal dispersion. For porous media, D_L is generally considered to be a function of advective velocity and pore structure. For fractured rock, both experimental evidence (Neretnieks, 1985) and numerical modelling studies (Dverstorp *et al*, 1992) indicate that D_L may also depend upon the transport distance, *i.e.*, D_L is scale-dependent.

Surface sorption refers to the sorption of dissolved radionuclide species onto the rock surface that is instantaneously accessible to advecting radionuclides, within the flowing fracture system. For the purposes of predicting transport of sorbing radionuclides, surface sorption is often assumed to be linear, reversible, instantaneous-equilibrium sorption. Thus at any given point and any given instant, there is a fixed ratio between the radionuclide's sorbed concentration C_s [mol/kg rock] in the rock and its dissolved concentration C_w [mol/m^3 water] in the pore water:

$$\frac{C_s}{C_w} = K_d \qquad (4)$$

This ratio is assumed to hold regardless of the transport system's history. The constant K_d is termed the mass distribution coefficient, and has units of m^3 (water)/kg (rock). For fractured rock, in defining the sorbed concentration C_s as above, it is implicitly assumed that a certain thickness δ [m] of the rock adjacent to each fracture interacts instantaneously with the pore water.

Alternatively the sorption process can be parameterized in terms of a surface sorption coefficient K_a [m] defined as c_s/C_w, where c_s [mol/m^2] is the number of moles of sorbed species per unit area of rock surface. K_d is related to K_a as $K_d = K_a/\delta\rho_s$, where ρ_s [kg/m^3] is the rock density.

Surface sorption results in a retardation of radionuclide transport, due to the temporary "storage" of radionuclides in sorbed state as the solute concentration increases, and release into solution (desorption) of the "stored" radionuclides as the solute concentration decreases. When this effect is included in the advection-dispersion equation, the modified transport equation may be written as:

$$R\frac{\partial C}{\partial t} = D_L\frac{\partial^2 C}{\partial x^2} - u\frac{\partial C}{\partial x} \tag{5}$$

where $R = 1 + K_a a_w$ is the retardation coefficient (dimensionless), and a_w [m^{-1}] is the available wetted surface per unit volume of water [m^2 (rock surface) /m^3 (water)]. The effect of sorption on radionuclide transport is seen as a retardation in the median velocity of the solute front, so that the retarded median velocity of the solute front is $u' = u/R$.

The term **matrix diffusion** refers to the gradual penetration by radionuclides into the matrix rock adjacent to a fracture, by diffusion through micropores in the rock. The retardation due to matrix diffusion and sorption deep within the rock matrix can be significantly greater than that due to the relatively instantaneous sorption at fracture surfaces (Moreno *et al.*, 1995). Matrix diffusion is usually modelled by solving a coupled system of two partial differential equations. The first equation is formed by adding a transfer term to the modified advection-dispersion equation:

$$R\frac{\partial C}{\partial t} = D_L\frac{\partial^2 C}{\partial x^2} - u\frac{\partial C}{\partial x} + a_w\theta_m D_m\left(\frac{\partial C_m}{\partial w}\right)_{w=0} \tag{6}$$

where $C_m(w,t)$ is the concentration in the pore water in the rock matrix, as a function of time t and distance w into the matrix from the fracture, θ_m is the porosity of the matrix rock, and D_m is the diffusion coefficient within the pore water in the matrix. The second equation describes one-dimensional diffusion within the rock matrix:

$$\frac{\partial C_m}{\partial t} = \frac{D_m\theta_m}{K_d\rho_m}\frac{\partial^2 C_m}{\partial w^2} \tag{7}$$

The form of the latter equation may vary depending upon assumptions concerning the geometry of matrix blocks. The form given is for matrix diffusion from a planar fracture.

Radioactive decay results in time-dependent transformation from any given radionuclide species to its daughter products, governed by the decay constant λ for the particular species. The effects of radioactive decay on transport of a specific radionuclide i are modelled by adding a concentration-dependent "source" term representing decay of its parent (species i-1), and subtracting a concentration-dependent "sink" term representing decay of species i in the advection-diffusion equation to give:

$$R_i \frac{\partial C_i}{\partial t} = D_L \frac{\partial^2 C_i}{\partial x^2} - u \frac{\partial C_i}{\partial x} + a_w \theta_m D_{mi} \frac{\partial C_{mi}}{\partial w}\Big|_{w=0} + \lambda_{i-1} R_{i-1} C_{i-1} - \lambda_i R_i C_i \quad (8)$$

where the subscripts i and i-1 indicate quantities which are specific to each particular radionuclide species. Similar "source" and "sink" terms must be included in the coupled, one-dimensional matrix diffusion equation:

$$R_{mi} \frac{\partial C_{mi}}{\partial t} = D_m \frac{\partial^2 C_{mi}}{\partial w^2} + \lambda_{i-1} R_{m,i-1} C_{m,i-1} - \lambda_i R_{mi} C_{mi} \quad (9)$$

where R_{mi} is the retardation coefficient for retardation of the ith species in the rock matrix, defined as:

$$R_{mi} = 1 + \frac{K_{di} \rho_m}{\theta_m}$$

The overall radionuclide transport for a given decay chain is calculated by simultaneously solving the above system of equations for all species $i = 1, 2, ..., N$, where N is the number of distinct species in the decay chain. For SITE-94, this calculation is carried out using the computer code CRYSTAL (Worgan and Robinson, 1995).

2.3.2 Characteristic parameters

In scoping calculations using the 1-D far-field performance-assessment code CRYSTAL, two parameter groups were found to fully characterize the hydrogeological factors that affect transport of radionuclides to the biosphere (SKI, 1996). These controlling factors are the Peclet number *Pe* [-], defined as:

$$Pe = \frac{qL}{\theta D_L} \tag{11}$$

and the F ratio *F* [s/m] defined as:

$$F = \frac{a_r L}{q} \tag{12}$$

where q [m/s] is Darcy velocity, L [m] is the transport distance from the radionuclide source to the discharge point, θ [-] is the effective porosity along the discharge path, D_L [m^2/s] is the effective longitudinal dispersion coefficient, and a_r [m^{-1}] is the specific surface (fracture surface area per unit rock volume), which is related to a_w as $a_r = \theta a_w$.

The Peclet number characterizes the relative importance of advection versus dispersion, while the F ratio partly characterizes the relative importance of sorption and matrix diffusion versus advection. High Peclet numbers imply that advective transport is dominant in relation to dispersion. High F ratios imply high surface areas available for sorption and matrix diffusion, in relation to advection of solute, and hence the possibility for high retardation of sorbing species (depending upon effective sorption coefficients, which vary among radionuclide species and depending upon geochemical conditions).

The scoping calculations with CRYSTAL (SKI, 1996) showed that the peak far-field release of radionuclides is essentially a function of *F* and *Pe*, with *F* being by far the more important factor (Figure 2.1). Low *F* gives high release rates, as does low *Pe*. The scoping calculations indicate that *Pe* influences the peak release mainly in the case of high *F* (high surface area relative to advective velocity), where it is observed that lower *Pe* (high dispersion

relative to advection) gives reduced retardation. It should be noted that the specific influence of F and Pe on far-field release will depend upon the suite of radionuclides considered, their respective decay constants (half-lives), and their sorption properties in relation to the assemblage of minerals that they encounter along transport pathways, en route to the biosphere.

In calculating Pe and F for a variety of conceptual models, the above definitions can be difficult to use because of their dependence on Darcy velocity and porosity. Particularly when considering discrete fractures or channels, the definition of a "bulk volume" on which to base values of these quantities can be rather arbitrary. In such cases, practically any value of porosity can be obtained by varying the thickness of intact rock, adjacent to the discrete conduits, that is considered to be included in the bulk volume V_b.

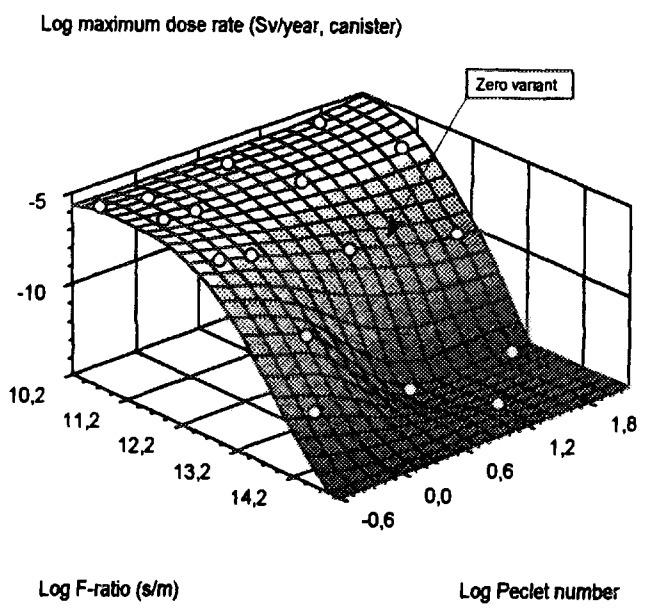

Figure 2.1 *Example plot of peak dose rate at the biosphere during the first 10^6 years after repository closure, as a function of the characteristic hydrogeological transport parameters F ratio and Peclet number (from SKI, 1996). The peak dose rate is defined as the maximum radiation dose rate to humans, in Seiverts per year, due to direct and indirect intake from a domestic well on Äspö. The example given is for Ra-226 and a near-field, single-canister source term corresponding to the SITE-94 Reference Case, Zero Variant. The ranges of F ratio and Peclet number correspond to approximate ranges of uncertainty and spatial variability in far-field transport properties, as determined by the hydrogeological evaluation in SITE-94 (from SKI, 1996).*

However, Pe and F for a given conduit can be expressed independently of assumptions regarding bulk volume, as:

$$Pe = \frac{uL}{D_L} = \frac{L}{\alpha_L} \tag{13}$$

and:

$$F = \frac{a_w L}{u} \tag{14}$$

where α_L is the longitudinal dispersivity and a_w is the specific surface (fracture surface area per unit volume of water). These expressions follow directly from the definitions above, and the fact that $q = \theta u$ and $a_r = \theta a_w$. From the latter expression, it is seen that F is the product of the available wetted surface (per unit water volume) times the advective transit time (L/u).

The above expressions for F and Pe, in terms of intrinsic properties of the conduits themselves (and independent of assumptions about what rock volume is to be associated with a given conduit) are useful in the present analysis which aims to evaluate these quantities for explicit, idealized models of pore geometry within distinct conduits. The alternative expressions in terms of q and a_r, as given in Equations 10 and 11, may be more useful in estimating these parameters from actual field data, should the actual field measurements be more directly related to the latter quantities. Furthermore, if either pair of basic quantities (u and a_w, or q and a_r) can be obtained directly from the field measurements or mathematical model at hand, there is no need to know the actual porosity in order to predict transport of sorbing radionuclides.

The F ratio is used in the present analysis, along with Darcy velocity, as a key indicator of far-field geosphere performance in terms of the geologic-barrier function. The following approximate ranges can be set forth based upon the results of consequence calculations in SITE-94 :

$F < 10^4$ yr/m	Low F-ratio (poor far-field performance). Retardation of the most significant radionuclides by the far-field geological barrier is negligible, resulting in high peak radiation doses to the biosphere.
10^4 yr/m $< F < 6x10^5$ yr/m	Intermediate F-ratio (intermediate far-field performance). The far-field geological barrier moderately retards radionuclide transport.
$F > 6x10^5$ yr/m	High F-ratio (good far-field performance). The far-field geological barrier retards most radionuclides sufficiently that peak releases of radiation to the biosphere are small.

These ranges should be viewed as a rough indication of far-field geosphere performance for radionuclide source terms and geochemical conditions similar to the SITE-94 Reference Case (SKI, 1996). It is emphasized that different source terms or geochemical conditions could lead to different ranges.

Regardless of whether F is expressed in terms of a_r and q, or in terms of a_w and u, there is a question as to whether the effective value of F for a given, heterogeneous transport path will be correctly estimated by evaluating each of these parameters independently. The scoping calculations with CRYSTAL, as mentioned above, considered only simple, 1-D transport pathways with uniform hydrologic and sorption properties along the pathway. In the present, simple evaluation only an idealized class of 1-D transport pathways is considered (as described in the following section), and hence the analysis is consistent with the CRYSTAL calculations. Since a wide range of such pathways, including extreme cases, are considered, the approach can be expected to yield valid, albeit wide bounds on geosphere performance. However, the issue of effective averages would need to be addressed, in any attempt to refine this analysis by considering more realistic, complex pathways for transport, or by making use of appropriate field data, if it existed.

2.3.3 Alternative assumptions for pore geometry

In the parameter groups F and Pe, which largely control the hydrogeological aspects of far-field performance, several terms appear which are strongly dependent upon the geometry of the pore space within the fractured rock. In particular, F depends on the Darcy velocity q and specific flow wetted surface a_r, or equivalently on the advective velocity u and the wetted surface per unit volume of water a_w, which are functions of both local pore geometry and network effects. Pe depends upon the longitudinal dispersivity α_L, which is a function of network effects. These quantities are difficult to measure directly in the field, and must be interpreted from field data based on an assumed conceptual model for transport geometry. Moreover, these quantities may be highly variable within a given site, and hence it may be necessary to predict ranges of values by extrapolation from models based on specific assumptions, *e.g.* discrete-fracture-network or channel-network models. Due to a shortage of unambiguous field experiments, the validity of any particular conceptual model of pore geometry in fractured rock is uncertain.

For the Äspö site, which is the main focus of the present analysis, the only available data that are relevant to estimation of transport parameters are a few (5) tracer tests. Nonsorbing tracers were used exclusively, in all of these tests. Such tests do not provide constraints on wetted surface, and give only indirect information on porosity (The latter is not really necessary for the evaluation of transport for sorbing species, but is used for comparisons among different conceptual models in SITE-94). Therefore, a wide range of possible relationships among flow and transport properties must be considered. In order to evaluate the consequences of this range of possibilities, these scoping calculations consider a variety of models for pore geometry.

The following simple models (see Figure 2.1) account for a wide variety of pore geometries:

A. **Simple planar fracture.**

B. **Simple tubular channels.**

C. **Multiple planar fractures.**

D. **Stepped fracture flowing "with the grain,"** in which the aperture varies between two values, b_1 and b_2, in the direction perpendicular to the direction of flow.

E **Stepped fracture flowing "across the grain,"** in which the aperture varies between two values along the direction of flow.

F **Crushed zone,** modelled as a planar fracture that is filled with well-packed, spherical grains of uniform radius.

Derivations of effective hydrologic parameters for each of these models are given in Appendix A, and summarized in Table 2.1. For purposes of comparison, the parameters for all models are expressed in Table 2.1 in terms of the parameters for Model A, the simple planar fracture, for the case when all models are constrained to yield the same Darcy velocity for a given hydraulic gradient (*i.e.* they are constrained to have the same net transmissivity or hydraulic conductivity). The expressions in Table 2.1 thus express differences among the models solely as a function of different assumptions on pore geometry, for which field data are lacking.

Model A is used as a point of reference only because it is conceptually and algebraically the simplest of the models, and in a strictly mathematical sense it is the most directly and uniquely related to transmissivity, a parameter for which considerable data are available. It should be emphasized that constant-aperture fractures such as represented by Model A are not representative of the vast majority of the fractures encountered in crystalline rock at repository depths. Most natural fractures display variations in aperture which are sufficient to cause large deviations from the relationships among parameters (as given in Table 2.1) that are predicted based on Model A. The other models that include aperture variation or channeling effects, although still highly simplistic, may be viewed as more representative of actual fractures.

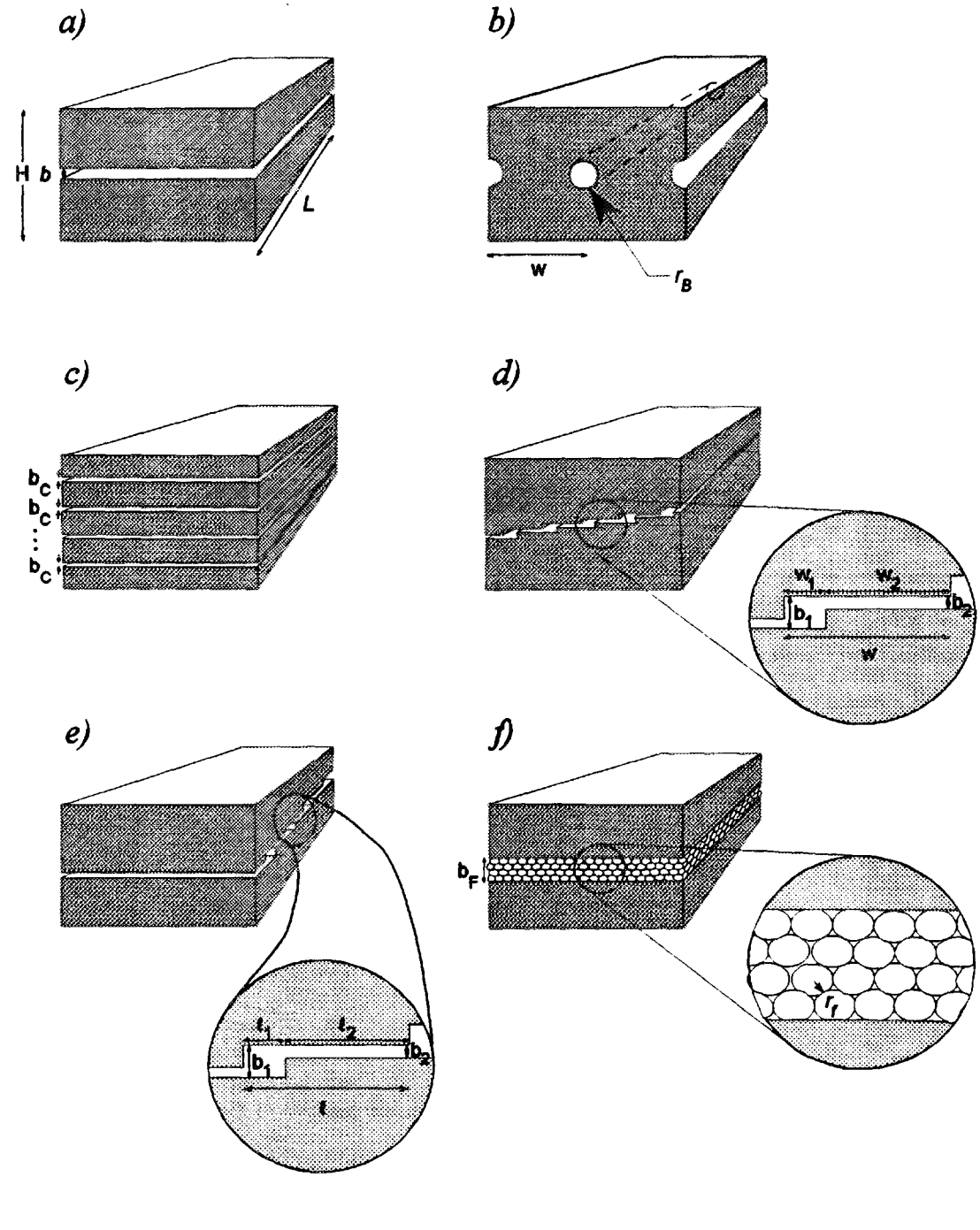

DWG0090c

Figure 2.2. Simple models for pore geometry including (a) simple planar fracture, (b) simple tubular channels, (c) multiple planar fractures, (d) stepped, "longitudinal-grain" fracture in which the aperture varies between two values, b_1 and b_2 in the direction perpendicular to the direction of flow, (e) stepped, "transverse-grain" fracture in which the aperture varies along the direction of flow, (f) crushed zone modelled as a planar fracture filled with well-packed, spherical grains of uniform radius. The direction of flow is into the page in all cases.

Model A: Simple planar fracture

Model A consists of a single, smooth planar fracture with two parallel faces, separated by an aperture b, and embedded in an effectively impermeable matrix (Figure 2.2a). This model, commonly referred to as a "parallel-plate" fracture, is used here as a reference model for comparisons with the other models of pore geometry. The transmissivity of the fracture is:

$$T_A = c b^3 \tag{15}$$

where:

b = fracture aperture [m]

c = $\rho_w g/12\mu_w \approx 8.2\text{x}10^5$ $m^{-1}s^{-1}$ at 20° C

ρ_w = density of water ≈ 1000 kg/m^3

g = gravitational acceleration ≈ 9.81 m/s^2

μ_w = viscosity of water ≈ $1.0\text{x}10^{-3}$ kg $m^{-1}s^{-1}$ at 20° C

Expressions for mean fluid velocity, specific wetted surface (per unit volume of water) and F-ratio for this model are, as developed in Appendix A:

$$u_A = c b^2 \frac{\Delta h}{L} \tag{16}$$

$$a_{w_A} = \frac{2}{b} \tag{17}$$

$$F_A = \frac{2L^2}{c b^3 \Delta h} \tag{18}$$

Equivalent porous-medium properties for a simple planar fracture are dependent upon the arbitrary choice of what matrix thickness to associate with the fracture. Different values may be appropriate depending upon the intended use of the parameters. Here, and for the other pore geometry models which follow, a very simple model for the fractured rock mass is assumed, which consists of a set of parallel, through-going fractures with identical aperture and uniform spacing H. For this simple model, the equivalent hydraulic conductivity for the rock mass is $K_A = cb^3/H$, the porosity is $\theta_A = b/H$, and the wetted surface per unit volume of rock mass is $a_r = 2/H$.

Model B: Simple tubular channels

Model B (Figure 2.2b) consists of a set of co-planar, tubular channels, spaced a uniform distance w apart, and having a cross-sectional radius r_B. This model may be thought of an extreme case of channelized flow. The equivalent transmissivity of the channelized plane (in the direction of the channels) is, as derived in Appendix A.2:

$$T = \frac{\frac{3}{2}\pi c r^4}{w} \tag{19}$$

When the transmissivity of the channelized plane represented by Model B is constrained to equal that of the simple, planar-fracture model (Model A) with aperture b, the required channel radius r_B can be calculated as a function of w and b, as given in the appendix. The resulting relationships between key transport parameters for this model and those for the simple, planar-fracture model are given in Table 2.1.

Model C: Multiple planar fractures

Model C (Figure 2.2c) is an idealized fracture zone consisting of n planar fractures, each of identical aperture equal to b_C. The net transmissivity is:

$$T = n c b_C^3 \tag{20}$$

If T is constrained to equal T_A, then the apertures b_C must be:

$$b_C = n^{-1/3} b \tag{21}$$

The resulting relationships between key transport parameters for this model and for an equivalent, simple planar fracture are given in Table 2.1.

Model D: Stepped fracture flowing with the grain

Model D (Figure 2.2d) is a very simple example of a variable-aperture fracture, produced by lateral offset of one surface of a stepped fracture, so that the resulting aperture varies between two values, b_1 and b_2. Flow occurs in the direction parallel to the steps ("with the grain"),

so that aperture is constant along any given streamline, and aperture varies between streamlines. The spacing between steps is uniformly equal to w, and the offset perpendicular to the steps is w_1. From geometrical considerations $0 < w_1 < w$. The aperture prior to offset is b_2, and the offset results in an increased aperture $b_1 > b_2$ in the w_1 -wide gap created by the offset.

The effective transmissivity of this model, in the flow direction, is derived in Appendix A.4 by treating each segment of the fracture as a distinct, parallel-plate conduit, and by ignoring any edge effects that may occur near each step. The net transmissivity when these segments act as conduits in parallel is:

$$T = (\omega \beta^3 + 1 - \omega) c b_D^3 \qquad (22)$$

where $b_D = b_2$, $\omega = w_1/w$ and $\beta = b_1/b_2$. From this, an expression for b_D in terms of b, the aperture for an equivalent, simple planar fracture (Model A), is readily obtained for the case $T = T_A$ as:

$$b_D = (\omega \beta^3 + 1 - \omega)^{-1/3} b \qquad (23)$$

The resulting relationships between key transport parameters for this model and for an equivalent, simple planar fracture are given in Table 2.1.

As β becomes large, flow through the fracture is predominantly through the w_1 wide by b_1 thick "channels," while advective velocities in the w_2 wide by b_2 thick segments of the fracture become negligible. At some point, only the surface area of the "channels" can be regarded as in contact with the advecting radionuclides, while the fracture surface area in the nearly-closed segments is essentially accessible to radionuclides only by diffusion from the active channels, at a rate comparable to ordinary matrix diffusion.

To account for this reduction in directly-accessible surface, the flow wetted surface area a_w and F for Model D are calculated using two different sets of formulae (as given in Table 2.1), one of which applies when b_2 is greater than a threshold value, b_{lim}, and the other which applies when $b_2 \leq b_{lim}$. The assumption of a particular value for the threshold b_{lim} is obviously a simplification, as in reality there will be a gradual transition from advective to dispersive-dominated transport in the small-aperture segments. Moreover, for reactive species

the nature of this transition will be controlled by species-dependent sorption effects, fracture mineralogy, and other geochemical conditions.

Model E: Stepped fracture flowing across the grain

Model E (Figure 2.2e) is similar to Model D, except that the aperture varies along the direction of flow. The model represents an idealized, stepped fracture, with a uniform spacing between steps of l, and an offset l_1 perpendicular to the steps. From geometrical considerations $0 < l_1 < l$. As for Model D, the aperture prior to offset is b_2, and the lateral offset of one side of the fracture results in an increased aperture $b_1 > b_2$ in the l_1 -wide gap created by the offset.

The effective transmissivity of this model, in the flow direction, is derived in Appendix A.5 by treating each segment of the fracture as a distinct, parallel-plate conduit, and by ignoring any edge effects that may occur near each step. The net transmissivity when these segments act as conduits in series is:

$$T = \left(\frac{\lambda}{\beta^3} + 1 - \lambda \right)^{-1} c b_E^3 \tag{24}$$

where $b_E = b_2$, $\lambda = l_1/l$ and $\beta = b_1/b_2$. From this, an expression for b_E in terms of b, the aperture for Model A, is readily obtained for the case $T_E = T_A$ as:

$$b_E = \left(\frac{\lambda}{\beta^3} + 1 - \lambda \right)^{1/3} b \tag{25}$$

The resulting relationships between key transport parameters for this model and an equivalent, simple planar fracture are given in Table 2.1. In contrast to Model D (stepped fracture flowing with the grain), the entire surface area of the fracture for this model is directly accessible to the advective flow, regardless of the value of β. This may be regarded as a somewhat unlikely situation, requiring that flow be forced through the less transmissive parts of the fracture by confining boundary conditions. A more realistic condition would be intermediate to the behaviors represented by the two stepped-fracture models.

Model F: Crushed zone/porous medium

Model *F* (Figure 2.2f) consists of a planar zone or fracture of aperture b_F, which is filled with spherical grains of uniform radius r_f. This model is an idealized representation of a strongly crushed zone, giving relatively high specific surface and porosity values for any transmissivity. The effective transmissivity of this model is derived in Appendix A.6, making use of the Carman-Kozeny equation (see Bear, 1972) to calculate the permeability of the packed spheres. This gives:

$$T = \frac{4}{15} \frac{\phi^3 r_f^2}{(1-\phi)^2} c\, b_F \tag{26}$$

where ϕ is the porosity of the packed spheres, which depends upon the type of packing (*e.g.* for hexagonal packing, $\phi = 1 - \pi/3\sqrt{2}$). For a given b_F and ϕ, the sphere radius required to satisfy $T = T_A$ is:

$$r_f = \frac{(1-\phi)b}{2\phi} \left(\frac{15}{\phi} \frac{b}{b_F} \right)^{1/2} \tag{27}$$

The resulting relationships between key transport parameters for this model and an equivalent, simple planar fracture are given in Table 2.1.

Table 2.1. Key transport parameters for the pore-geometry models A through F. Parameters for Models B through F are expressed in terms of the parameters for Model A to facilitate comparison with the parallel-plate fracture model. The row labelled D gives formulae for the general case of Model D. The row labelled D_1 gives approximate formulae for the case of Model D where $b_D < b_{lim}$

	u	a_w	F	θ
A	$u_A = cb^2\frac{\Delta h}{L}$	$a_{w_A} = \frac{2}{b}$	$F_A = \frac{2L^2}{cb^3\Delta h}$	$\theta_A = \frac{b}{H}$
B	$\sqrt{\frac{3}{2}\frac{w_B}{\pi b}}\,u_A$	$\left(\frac{3}{2}\frac{\pi b}{w_B}\right)^{1/4} a_{w_A}$	$\left(\frac{2}{3}\right)^{1/4}\left(\frac{\pi b}{w_B}\right)^{3/4} F_A$	$\sqrt{\frac{2}{3}\frac{\pi b}{w_B}}\,\theta_A$
C	$n^{-2/3}u_A$	$n^{1/3}a_{w_A}$	nF_A	$n^{2/3}\theta_A$
D	$\frac{(\omega\beta^3+1-\omega)^{1/3}}{\omega\beta+1-\omega}\,u_A$	$\frac{(\omega\beta^3+1-\omega)^{1/3}+(\beta-1)\frac{b}{w}}{\omega\beta+1-\omega}\,a_{w_A}$	$\left(1+\frac{(\beta-1)\frac{b}{w}}{(\omega\beta^3+1-\omega)^{1/3}}\right)F_A$	$\frac{\omega\beta+1-\omega}{(\omega\beta^3+1-\omega)^{1/3}}\,\theta_A$
D_1	$\omega^{-2/3}u_A$	$\left(\omega^{1/3}+\frac{1}{\omega}\frac{b}{w}\right)a_{w_A}$	$\left(\omega+\omega^{-1/3}\frac{b}{w}\right)F_A$	$\omega^{2/3}\theta_A$
E	$\frac{u_A}{(\lambda/\beta^3+1-\lambda)^{1/3}(\lambda\beta+1-\lambda)}$	$\frac{(\lambda/\beta^3+1-\lambda)^{-1/3}+(\beta-1)\frac{b}{l}}{\lambda\beta+1-\lambda}\,a_{w_A}$	$\left[1+(\beta-1)\left(\frac{\lambda}{\beta^3}+1-\lambda\right)^{1/3}\frac{b}{l}\right]F_A$	$(\lambda/\beta^3+1-\lambda)^{1/3}(\lambda\beta+1-\lambda)\,\theta_A$
F	$\left(\frac{b}{\phi b_F}\right)u_A$	$\frac{1}{1-\phi}\sqrt{\frac{3}{5}\frac{\phi b_F}{b}}\,a_{w_A}$	$\frac{1}{1-\phi}\sqrt{\frac{3}{5}\left(\frac{\phi b_F}{b}\right)^3}\,F_A$	$\left(\frac{\phi b_F}{b}\right)\theta_A$

3 Simple predictions of groundwater flow

The simple evaluation of groundwater flux is based on the hydrologic model described in Section 2.2, for Äspö and seven other study sites (Finnsjön, Sternö, Klipperås, Gideå, Fjällveden, Svartboberget, and Kamlunge) for which information are available from surface and borehole investigations carried out by SKB. Each site is assumed to contain a repository through which groundwater flows and eventually discharges at a point on the ground surface. Groundwater occurs through the host rock of the repository which may consist in part of rock mass, fractures and fracture zones, and the disturbed-rock zone (DRZ) which is formed around repository tunnels by excavation and operation of the repository (see Winberg, 1991).

For each site, calculations require selection of hydraulic conductivities and hydraulic gradients. These are selected according to the following strategy.

The geometry of flow paths from the repository to the discharge point are based upon consideration of SKB's interpretations of the configuration of fracture zones at the sites (Ahlbom *et al.*, 1991ab; 1992abc; Andersson *et al.* 1991; Gentzschein, 1986; Wikberg *et al.*, 1991). The general aim has been to postulate a plausible set of transport pathways that lead to a broad range of flux estimates, within the constraints of the assumed structural models. No attempt has been made to evaluate uncertainty in the structural interpretations themselves.

Gradients are selected in one of two ways.

1) The maximum local head in the site is transmitted relatively undiminished to the repository, and the minimum local head is transmitted to the repository discharge point. The discharge point is either a fracture zone separated from the repository by 10 m to 100 m of rock mass or is the ground surface. This results in the maximum possible gradient through the repository, under present climatic and surface conditions.

2) The regional gradient applies at repository depth. This is the most hydrologically reasonable and simple assumption, which would not require anomalous configurations of fractures and surface conditions.

Hydraulic conductivities along the flow path from the repository to the discharge point are selected in one of two ways.

1) For flow from the repository to a discharge point through only the rock mass, the hydraulic conductivity along the flow path is the same as that of the rock mass at repository depth. This results in a minimal estimate of the groundwater flux for a given gradient at the site.

2) For flow from the repository via the disturbed-rock zone, and/or fracture zones connecting in series to a surface discharge point, the fracture zone hydraulic conductivity at repository depth applies along the entire flow path.

Only a few combinations of these conditions need be considered to determine plausible ranges of flux and to illustrate uncertainties inherent in these systems.

With regard to hydraulic conductivity, the calculations assume repository-depth conductivity along the entire transport path to the discharge point, although in some cases data may indicate that hydraulic conductivity increases by a few orders of magnitude towards the surface. This results in relatively low estimates of flux compared with using an increasing conductivity along the flow path.

3.1 Evaluation of groundwater flow at the Äspö site

The basis for analysis of the Äspö site is provided by the pre-investigations for the Äspö Hard Rock Laboratory (HRL). The scope of the pre-investigations, as described by Stanfors *et al.* (1991), was relatively intensive in comparison with the other study sites considered herein. The "siting" stage of the pre-investigations included airborne geophysical surveys, interpretation of topographic lineaments, and geological mapping over a regional (25-35 km) scale. This was followed by a "site-description" stage, during which geological and geophysical investigations were conducted at the surface, on a local (2-3 km) scale, and an extensive suite of geoscientific investigations were performed in a total of 27 shallow percussion-drilled and four deep, core-drilled boreholes. Finally, in the "prediction" stage eight more percussion-drilled holes and twelve more core-drilled holes were located in a smaller area of the site, and used for additional investigations to characterize hydrogeological structures around the HRL. Noteworthy data from these investigations include results of two long-term (2-3 month) hydrological pumping tests, during which groundwater pressures were measured in sections of nearly all of the boreholes. In the second of these tests, a radially convergent tracer test was performed in an attempt to characterize nonreactive transport in several major fracture zones.

3.1.1 Structural model of the site near the hypothetical repository

The geologic structural model employed for the Äspö site is the SKB conceptual model, based upon data from the Äspö pre-investigations (Wikberg *et al.*, 1991). At the time this simple evaluation was initiated, the SITE-94 structural model (Tirén *et al.*, 1996) was not yet available.

The hypothetical repository is located in Rock Mass Unit 2 (RMU-2) in the Southeastern part of Äspö (see Figure 4-9, Wikberg *et al.*, 1991). This is the same location as the Äspö HRL, but deeper. The repository area is bounded by four vertical or sub-vertical fracture zones; EW-3, NE-2, NNW-5, and NNW-1, which form the structural model (see Appendix 10, Gustafson *et al.*, 1991). In addition, the NE-1 zone is included in the analysis, as it may penetrate the repository area if it extends to repository depth. The hydraulic properties of these features are listed in Table 3.1.

Table 3.1. Hydraulic conductivity or transmissivity of relevant features at Äspö, according to Wikberg et al. (1991). K_g denotes geometric mean.

Unit	Best estimate	Range
Rock mass		
RMU-2	K_g = 1.0 x 10^{-10} m/s	
Fracture zones		
EW-3	T = 5.0 x 10^{-7} m^2/s	1 x 10^{-7} - 1 x 10^{-6} m^2/s
NE-2	T = 4.0 x 10^{-6} m^2/s	2 x 10^{-6} - 1 x 10^{-5} m^2/s
NNW-5	T = 5.0 x 10^{-5} m^2/s	1 x 10^{-5} - 1 x 10^{-4} m^2/s
NNW-1	T = 1.5 x 10^{-5} m^2/s	5 x 10^{-6} - 2 x 10^{-5} m^2/s
NE-1	T = 2.0 x 10^{-4} m^2/s	4 x 10^{-5} - 4 x 10^{-4} m^2/s

3.1.2 Position and design of the repository

Because of the richness of fracturing below Äspö at all scales, it appears difficult to locate a full-scale SKB-91/KBS-3 repository at this site. In fact, it is difficult to locate even a small repository having a 100 m set-back from major hydraulically-active zones, as proposed by SKB (1992). The hypothetical repository used in this analysis is therefore only 1% of the SKB 91 design capacity (50 canisters) and is located at a depth of 600 m, between the fracture zones mentioned above. This location is below a seismic reflection at 300 to 500 m which may indicate an otherwise undetermined sub-horizontal hydraulically active zone (Wikberg *et al.*, 1991, p. 32). This repository covers an area of 150 x 150 m^2.

3.1.3 General assumptions

The hydraulic gradient at repository depth below Äspö may derive either from regional or local differences in water table elevation. Considering local topographic conditions, the maximum head on Äspö is about +2 m.a.s.l. based on the water table elevation above sea level (Figure 3.34, Wikberg *et al.*, 1991) at the present time.

However, within a few thousand years coastal regression (resulting from post-glacial isostatic rebound) will cause Äspö to become a hill on the mainland, and the local differences in

water table elevation may be between +10 m and +20 m. This head difference may be transmitted to repository depth. It is difficult to predict the direction of the gradient, if local conditions should prevail at depth. However, it is possible that a strong local circulation cell may develop, bringing locally recharged water to repository depth, and bringing repository fluids to a local discharge point. Considering regional topography, the maximum regional water table elevation within 5 km west of Äspö is about 10 m.a.s.l. If this hydraulic head were transmitted undiminished through major sub-horizontal zones, then the maximum possible head at repository depth would be about +10 m. In a relatively homogeneous regional model of Äspö (Gustafson *et al.*, 1989), the predicted head at -500 m is about +2 m.

Thus a reasonable range of excess head at repository depth is from +1 m to +10 m. Because Äspö is located at the coast, water at repository depths is likely discharging. Thus the hydraulic gradient under today's climatic and surface conditions, even in the salt water found at depth, is likely directed upwards at some angle (Voss and Andersson, 1993; Provost *et al.*, 1996). The present analysis assumes that the hydraulic gradient at repository depth is directed vertically upward with a magnitude of from 1 m to 10 m per 600 m.

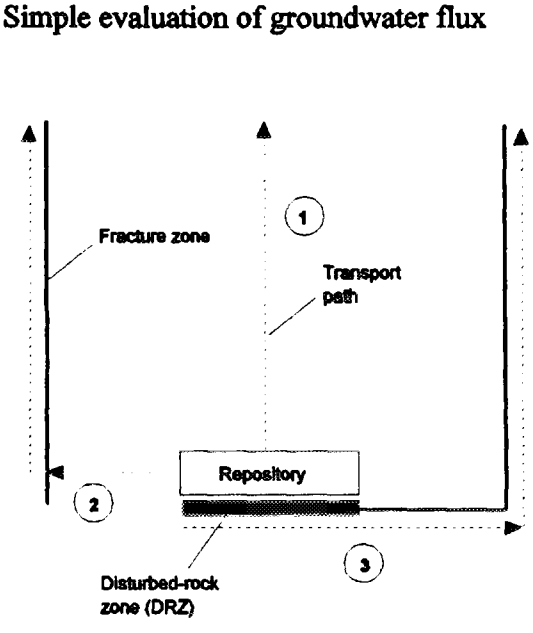

Figure 3.1. Schematic view of the different cases evaluated for the Äspö site.

3.1.4 Flow calculations

3.1.4.1 Case 1: Transport through rock mass to surface

Set-up

Transport is vertically upward through the rock mass (Figure 3.1). The distance to the surface is about 600 m.

Results

For Δh = 10 m:

$$q = (10^{-10} \text{ m/s})\ (10 \text{ m}/600 \text{ m}) = 1.7 \times 10^{-12} \text{ m/s} = 5.4 \times 10^{-5} \text{ m/yr}$$

For Δh = 1 m:

$$q = 1.7 \times 10^{-13} \text{ m/s} = 5.4 \times 10^{-6} \text{ m/yr}$$

3.1.4.2 Case 2: Transport through rock mass to discharging fracture zone

Set-up

Transport is through 10 m of rock mass to a discharging major fracture zone. There is effectively no delay in the fracture zone for transport to the surface. This case may represent the situation where the near-field rock acts as a barrier, whereas the far-field has no isolating effect.

Results

For Δh = 10 m:

$$q = (10^{-10} \text{ m/s})(10 \text{ m}/10 \text{ m}) = 1.0 \times 10^{-10} \text{ m/s} = 3.2 \times 10^{-3} \text{ m/yr}$$

For Δh = 1 m:

$$q = 1.0 \times 10^{-11} \text{ m/s} = 3.2 \times 10^{-4} \text{ m/yr}$$

3.1.4.3 Case 3: Transport through fracture zone to surface

Set-up

Transport occurs through the DRZ directly to a discharging major fracture zone. The DRZ has the same properties as the fracture zone, and acts to connect previously unconnected hydraulic conductors intersecting the hypothetical repository.

The thickness of the major fracture zone is b = 10 m. This is considered to be a maximum possible value for effective thickness, because flow is likely confined to a limited number of discrete fractures, and does not occur through a ten-meter wide porous medium. Use of this high value of thickness tends to decrease the calculated fluid flux.

Case 3a: Transport through zone NE-1 (most conductive zone)

Transmissivity of fracture zone: $T = 20 \times 10^{-5}$ m^2/s

Case 3b: Transport through zone EW-3 (least conductive zone)

Transmissivity of fracture zone: $T = 0.05 \times 10^{-5}$ m^2/s

Results

Case 3a: Transport through zone NE-1

$K = (20 \times 10^{-5}\ \text{m}^2/\text{s})/(10\ \text{m}) = 2.0 \times 10^{-5}$ m/s

For Δh = 10 m:

$$q = (2.0 \times 10^{-5}\ \text{m/s})(10\ \text{m}/600\ \text{m}) = 3.3 \times 10^{-7}\ \text{m/s} = 10.5\ \text{m/yr}$$

For Δh = 1 m:

$$q = (2.0 \times 10^{-5}\ \text{m/s})\ (1\ \text{m}/600\ \text{m}) = 3.3 \times 10^{-8}\ \text{m/s} = 1.05\ \text{m/yr}$$

Case 3b: Transport through zone EW-3

$K = (0.05 \times 10^{-5}\ m^2/s)/(10\ m) = 5.0 \times 10^{-8}\ m/s$

For $\Delta h = 10$ m:

$$q = (5.0 \times 10^{-8}\ m/s)(10\ m/600\ m) = 8.3 \times 10^{-10}\ m/s = 2.6 \times 10^{-2}\ m/yr$$

For $\Delta h = 1$ m:

$$q = (5.0 \times 10^{-8}\ m/s)\ (1\ m/600\ m) = 8.3 \times 10^{-11}\ m/s = 2.6 \times 10^{-3}\ m/yr$$

3.2 Evaluation of groundwater flow at the Finnsjön site

The basis for analysis of the Finnsjön site is provided by the site-investigation activities (1977-1983), and the SKB Fracture Zone Project (1985-1992), as described by Ahlbom *et al.* (1992c) and Andersson *et al.* (1991). The scope of the former was similar to the "siting" and "site-description" stages of the Äspö pre-investigations; airborne geophysical surveys, topographic lineament interpretations, and geological mapping were performed over a regional (25-35 km) scale, followed by geological and geophysical investigations on a local (2-3 km) scale, and an extensive suite of geoscientific investigations in a total of 17 shallow percussion-drilled and seven deep, core-drilled boreholes. Three more percussion-drilled holes and four core-drilled holes were used for detailed studies in the Fracture Zone Project, which was focused on the characterization of a major, gently dipping fracture zone referred to as Zone 2. Noteworthy data from these investigations include results of a series of tracer tests that were conducted within Zone 2.

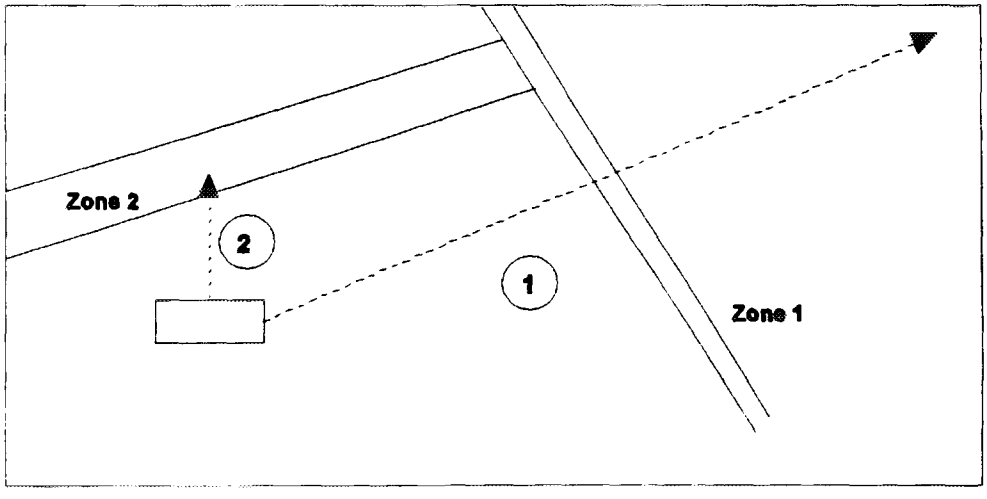

Figure 3.2. Schematic view of the different cases evaluated for the Finnsjön site.

3.2.1 General assumptions

The structural model of the site including geology (rock mass and fracture zone description) and location and design of the hypothetical repository are based on the SKB-91 analysis (see Figure 3.2). The hydraulic conductivity of the rock mass is 10^{-8} m/s at depth 600 m (from Figure 8-3, SKB, 1992). This is employed in the analysis although it is a low value, because according to SKB-91, hydraulic conductivity increases two orders of magnitude along a trajectory to the surface.

3.2.2 Calculations

3.2.2.1 Case 1: Transport laterally through the rock mass

Set-up

Transport occurs laterally through the rock mass according to typical trajectories for the SKB-91 reference case (Figure 9-6, part 3, SKB, 1992). The transport distance from repository to discharge point is approximately 5 km. The hydraulic head change over the trajectory, taken from a water table map (Figure 5-5, SKB, 1992), is approximately 15 m.

Results

$q = (10^{-8}\ \text{m/s})(15\ \text{m}/5000\ \text{m}) = 3.0 \times 10^{-11}\ \text{m/s} = 9.5 \times 10^{-4}\ \text{m/yr}$

3.2.2.2 Case 2: Transport upward through rock mass

Set-up

The gradient is directed upward through 100 m of rock mass, from the hypothetical repository to Zone 2. There is effectively no delay in Zone 2, for transport to surface. The excess hydraulic head below Zone 2 is up to +1 m, according to borehole measurements (Andersson *et al.*, 1991, Pages A4-A7).

Results

$q = (10^{-8}\ \text{m/s})(1\ \text{m}/100\ \text{m}) = 1.0 \times 10^{-10}\ \text{m/s} = 3.2 \times 10^{-3}\ \text{m/yr}$

3.3 Evaluation of groundwater flow at the Sternö site

The basis for analysis of the Sternö site is characterization activities performed between 1977 and 1979, as described by Ahlbom *et al.* (1992a). Geological and geophysical investigations at the surface were very limited relative to the investigations at Äspö and Finnsjön. A total of five deep, core-drilled boreholes and no percussion-drilled holes were used for subsurface geoscientific investigations.

3.3.1 General assumptions

Repository

The hypothetical repository is located at a depth of 600 m because of an apparent decline in hydraulic conductivity below 400 m to 500 m depth (see Figure 14, Ahlbom *et al.*, 1992c). Given the few indications of fracture zones available, it appears possible to locate approximately 40% of a full-scale KBS-3/SKB 91 repository.

Hydraulic conductivity

The hydraulic conductivity is about 10^{-9} m/s for the rock mass at repository depth, and is about 10^{-6} m/s for fracture zones (Figure 14, Ahlbom *et al.*, 1992c). Only one of the fracture zones at the sites has been identified by a borehole. However, at least two of the five boreholes exhibit local hydraulic conductivities as high as the fracture zone. Thus other fractures or fracture zones, as yet unmapped, may exist at depth, which motivates the use of the higher conductivity for the calculation of Case 2 below.

Gradients

The maximum water table elevation at Sternö is +25 m, giving a maximum local gradient of about 25 m/km (p. 26, Ahlbom *et al.*, 1992c). The regional gradient, as defined by the regional topography, is about 3 m/km.

3.3.2 Flow calculations

Flux calculations

Case 1: Vertical discharge through the rock mass

Vertical, upward discharge occurs through the rock mass, from the repository to the surface. A head of +10 m at the repository is assumed, based on local topography. The high head is transmitted to the repository via a conductive fracture zone. Because of the lack of postglacial isostatic rebound at this location, no greater head differences are expected within the next few thousands of years.

$$q = (10^{-9} \text{ m/s})(10 \text{ m}/600 \text{ m}) = 1.7 \times 10^{-11} \text{ m/s} = 5.3 \times 10^{-4} \text{ m/yr}$$

Case 2: Discharge through a major fracture zone

Discharge occurs through a major fracture zone to the surface.

$$q = (10^{-6} \text{ m/s})(10 \text{ m}/600 \text{ m}) = 1.7 \times 10^{-8} \text{ m/s} = 5.3 \times 10^{-1} \text{ m/yr}$$

3.4 Evaluation of groundwater flow at the Klipperås site

The basis for analysis of the Klipperås site is characterization activities performed in 1984-1985, as described by Ahlbom *et al.* (1992b). Geological and geophysical investigations at the surface were more extensive than at Sternö, but more limited than the investigations at Äspö and Finnsjön. A total of fourteen deep, core-drilled boreholes and fourteen shallow, percussion-drilled holes were used for subsurface geoscientific investigations.

3.4.1 General assumptions

Repository

Assuming a hypothetical repository located at a depth of 900 m (100 m below the horizontal fracture zone H1) and bounded by the vertical or subvertical zones; 8, 4, 2, 30% of the full-scale KBS-3/SKB-91 inventory can be stored. The repository is divided in two parts by zone 5 (see Ahlbom *et al.*, 1992b).

Hydraulic conductivity

The hydraulic conductivity of the rock mass at repository depth is about 3 $x10^{-9}$ m/s and about 10^{-6} m/s for the most conductive fracture zones at depth (Gentzschein, 1986; Lindbom *et al.*, 1988).

Gradients

The maximum local gradient, based on the local topography, is about 20 m/ 4 km. The regional gradient as defined by the regional topography is about 5 m/ km. Thus the local and regional gradients are identical at this site.

3.4.2 Flow calculations

Case 1: Discharge through rock mass

Vertical flow occurs upward through the rock mass either to the nearby fracture zone H1 (100 m distant), or to the surface (900 m distant), or lateral flow occurs through the rock mass to the surface (any distance, *e.g.* 9 km). The regional/local head gradient applies.

$$q = (3 \times 10^{-9} \text{ m/s})(0.005) = 1.5 \times 10^{-11} \text{ m/s} = 4.7 \times 10^{-4} \text{ m/yr}$$

Case 2: Discharge through fracture zones

Vertical flow occurs upward through fracture zones (900 m to surface), or lateral flow occurs through fracture zones to the surface (any distance, *e.g.* 9 km). The regional/local head gradient applies.

$$q = (1.0 \times 10^{-6} \text{ m/s})(0.005) = 5.0 \times 10^{-9} \text{ m/s} = 1.6 \times 10^{-1} \text{ m/yr}$$

3.5 Evaluation of groundwater flow at the Gideå site

The basis for analysis of the Gideå site is characterization activities performed in 1981-1983, as described by Ahlbom *et al.* (1991b). The scope of geological and geophysical investigations at the surface was roughly comparable to that for Klipperås. A total of thirteen deep, core-drilled boreholes and 24 shallow, percussion-drilled holes were used for subsurface geoscientific investigations.

3.5.1 General assumptions

Repository

The hypothetical repository is located according to KBS-3, at a depth of 600 m (KBS, 1983, p. 18:29). However, it may not be possible to locate a full-scale KBS-3 type repository if high conductivity features are scattered throughout the rock mass as is discussed below.

Hydraulic conductivity

Due to the large and equally great variation in hydraulic conductivity in the rock mass and in fracture zones it is impossible to distinguish these hydrologically. In this case, rock type (*e.g.* granite gneiss, dolerite dikes and granitic dikes) may be as important as existence of fractures in determining conductive structures. Because of the lack of data below 600 m, a rock mass hydraulic conductivity of 10^{-8} m/s is chosen for calculations of flux. Inspection of the vertical conductivity distribution in the rock mass (Figure 21, Ahlbom *et al.*, 1991b) indicates that it may not be possible to locate a repository in a rock volume having less than the chosen value.

Gradients

The regional gradient as defined by the regional topography is about 100 m per 10 km. The maximum local water table gradient is about 20 m per km (Figure 18, Ahlbom *et al.*, 1991b). Measured heads at depth vary by as much as 5 m relative to the water table (Ahlbom *et al.*, 1991b, Figure 23).

3.5.2 Flow calculations

Case 1: Vertical discharge through the rock mass

Vertical discharge occurs through the rock mass from the repository to the surface. A head of +10 m at the repository, due to local topography, is assumed.

$$q = (10^{-8} \text{ m/s})(10 \text{ m}/600 \text{ m}) = 1.7 \times 10^{-10} \text{ m/s} = 5.3 \times 10^{-3} \text{ m/yr}$$

Case 2: Discharge through rock mass to the Gulf of Bothnia

Discharge is through the rock mass to the Gulf of Bothnia, ten kilometers away.

$$q = (10^{-8} \text{ m/s})(100 \text{ m}/10{,}000 \text{ m}) = 1.0 \times 10^{-10} \text{ m/s} = 3.2 \times 10^{-3} \text{ m/yr}$$

3.6 Evaluation of groundwater flow at the Fjällveden site

The basis for analysis of the Fjällveden site is characterization activities performed in 1981-1983, as described by Ahlbom *et al.* (1991a). The scope of geological and geophysical investigations at the surface was roughly comparable to that for Gideå and Klipperås. A total of fifteen deep, core-drilled boreholes and 49 shallow, percussion-drilled holes were used for subsurface geoscientific investigations.

3.6.1 General assumptions

Repository

The hypothetical repository is located according to KBS-3, at a depth of 500 m (KBS, 1983, p. 18:29). It may not be possible to locate a full-scale repository here because of repeated layers of highly conductive granite gneiss at the site (see Figure 13, Ahlbom *et al.*, 1991a).

Hydraulic conductivity

Due to the large and equally great variation in hydraulic conductivity in the rock mass and fracture zones it is impossible to distinguish these hydrologically. However, in this case it is apparent that the granite gneiss rock type has hydraulic conductivity which is two orders higher than the other major rock type (sedimentary gneiss). This hydraulic conductivity is even higher than that of fracture zones as interpreted by SKB. Thus the rock type may be more important than fractures in determining conductive structures. Hydraulic conductivity of sedimentary gneiss at repository depth is about 10^{-10} m/s, and about 10^{-8} m/s for granite gneiss. These values are chosen for calculations of flux.

Gradients

The regional gradient is defined by elevation of the site above the coast, and is about 50 m per 20 km. The local gradient of the groundwater table is a maximum of about 25 m per km (Figure 17, Ahlbom *et al.*, 1991a). Measured heads at depth vary as much 7 m relative to the water table (Ahlbom *et al.*, 1991a, Figure 23).

3.6.2 Flow calculations

Case 1: Vertical discharge through sedimentary gneiss to surface

Vertical discharge occurs through sedimentary gneiss from the repository to the surface. A head of +10 m at the repository, due to local topography, is assumed.

$$q = (10^{-10} \text{ m/s})(10 \text{ m}/500 \text{ m}) = 2.0 \times 10^{-12} \text{ m/s} = 6.3 \times 10^{-5} \text{ m/yr}$$

Case 2: Vertical discharge through granite gneiss to surface

Vertical discharge occurs through granite gneiss from the repository to the surface. A head of +10 m at the repository, due to local topography, is assumed.

$$q = (10^{-8} \text{ m/s})(10 \text{ m}/500 \text{ m}) = 2.0 \times 10^{-10} \text{ m/s} = 6.3 \times 10^{-3} \text{ m/yr}$$

3.7 Evaluation of groundwater flow at the Svartboberget site

The basis for analysis of the Svartboberget site is summarized the KBS-3 report (KBS, 1983). The scope of geological and geophysical investigations at the surface was more limited than for Gideå and Klipperås. A total of seven deep, core-drilled boreholes and sixteen shallow, percussion-drilled holes were used for subsurface geoscientific investigations.

3.7.1 General assumptions

Repository

The hypothetical repository is arbitrarily located at 500 m depth. It may not be possible to locate a full-scale repository here because of a large number of closely spaced fracture zones (KBS, 1983, p. 18:60).

Hydraulic conductivity

Due to the large and equally great variation in hydraulic conductivity in the rock mass and fracture zones it is difficult to distinguish these hydrologically. At depth, however, the fracture zones may have significantly higher conductivity than the rock mass (KBS, 1983, Figures 18-38 through 18-40). The hydraulic conductivity of the rock mass at repository depth is about 10^{-10} m/s, and is as high as 10^{-7} m/s in major fracture zones. These values are chosen for calculations of flux.

Gradients

The regional gradient is defined by elevation of the site above the coast, and is about 300 m per 100 km. Local gradient of the groundwater table is a maximum of about 50 m per km (KBS, 1983, Figure 18-34). The repository is located below a 50 m high hill.

3.7.2 Flow calculations

Flux calculations

Case 1: Discharge through rock mass

Lateral or vertical flow occurs through 500 m of rock mass from the repository to either the surface or a discharging fracture zone in which no delay occurs. A head of +50 m exists at the repository due to local topography, and a head of zero exists in the fracture zone.

$$q = (10^{-10}\ \text{m/s})(50\ \text{m}/500\ \text{m}) = 1.0 \times 10^{-11}\ \text{m/s} = 3.2 \times 10^{-4}\ \text{m/yr}$$

Case 2: Vertical discharge through major fracture zone

Vertical discharge occurs through a major fracture zone from the repository to the surface assuming a head of +10 m at the repository due to local topography.

$$q = (10^{-7}\ \text{m/s})(10\ \text{m}/500\ \text{m}) = 2.0 \times 10^{-9}\ \text{m/s} = 6.3 \times 10^{-2}\ \text{m/yr}$$

3.8 Evaluation of groundwater flow at the Kamlunge site

The basis for analysis of the Kamlunge site is characterization activities performed in 1981-1983, as described by Ahlbom *et al.* (1992a). The scope of geological and geophysical investigations at the surface was roughly comparable to that for Gideå and Klipperås. A total of sixteen deep, core-drilled boreholes and 22 shallow, percussion-drilled holes were used for subsurface geoscientific investigations.

3.8.1 General assumptions

Repository

The hypothetical repository is located according to KBS-3, at a depth of 450 m, which is 100 m above the horizontal H1-zone (KBS, 1983, Figure 18:30). About 70% of the full-scale KBS-3/SKB-91 inventory can be stored.

Hydraulic conductivity

The hydraulic conductivity of the rock mass at repository depth is about 10^{-10} m/s and about 10^{-8} m/s for a typical fracture zone.

Gradients

The local gradient is about 65 m/km and the local relief is on the order of 130 m (KBS, 1983, Figures 18-23). The regional gradient relative to the coast is roughly 3 m/km and is thus negligible relative to the local gradient.

3.8.2 Flow calculations

Case 1a: Downward discharge at low gradient

Downward discharge occurs through 100 m of rock mass from the repository to Zone H1. A head of +75 m is assumed to exist at the repository, due to local topography. A head of zero is assumed at H1.

$$q = (10^{-10} \text{ m/s})(75 \text{ m}/100 \text{ m}) = 7.5 \times 10^{-11} \text{ m/s} = 2.4 \times 10^{-3} \text{ m/yr}$$

Case 1b: Downward discharge at high gradient

This case is the same as Case 1a, except that a local gradient of 65 m/km is assumed to apply at repository depth.

$$q = (10^{-10} \text{ m/s})(0.065) = 6.5 \times 10^{-12} \text{ m/s} = 2.1 \times 10^{-4} \text{ m/yr}$$

Case 1c: Discharge through major fracture zone

This case is the same as Case 1a, except that discharge from the repository is assumed to occur through the disturbed zone or via channels to H1 or some other major fracture zone, to a discharge point at any distance.

$$q = (10^{-8} \text{ m/s})(0.065) = 6.5 \times 10^{-10} \text{ m/s} = 2.1 \times 10^{-2} \text{ m/yr}$$

3.9 Evaluation of results for Darcy velocity

Results for Äspö

The calculated ranges of Darcy velocity are shown in Table 3.2 and Figure 3.3. For the Äspö site, a low Darcy velocity for groundwater percolating through the hypothetical repository is obtained only for the unlikely case of upward flow through 600 m of undisturbed rock mass, without encountering fracture zones. In all of the cases with transport through less than 100 m of undisturbed rock, the calculated velocities are greater than 10^{-4} m/yr.

The calculated Darcy velocities provide a rough indication of geologic-barrier performance for the different cases, although other factors such as discharge-path length, wetted surface area, and geochemical properties of the rock and water can also exert strong influence on performance. Predictions of the geologic-barrier performance at Äspö, taking into account Darcy velocity, discharge-path length and wetted surface area, are presented in Chapter 4, based on the F ratio as defined in Section 2.3.2.

In Project-90 (SKI, 1991), radionuclide transport to the biosphere along one-dimensional pathways was assessed for different values of Darcy velocity, in combination other parameters affecting radionuclide transport. In these calculations, an effort was made to evaluate all meaningful combinations of Darcy velocity ranges with other important parameters. Based on these calculations, the following approximate classification was set forth to describe geologic-barrier performance as a function of Darcy velocity (denoted "flux" in Project-90):

Poor	10^{-2} m/yr
Intermediate	10^{-4} m/yr
Good	10^{-6} m/yr

"Poor" flux conditions imply high Darcy velocities and consequently poor performance of the geologic barrier. "Good" flux conditions imply low Darcy velocities and consequently good performance of the geologic barrier. "Intermediate" flux conditions (denoted "Normal" in Project-90) imply intermediate effectiveness of the geologic barrier.

Comparison of Äspö and Finnsjön sites

For Finnsjön, although the hydraulic conductivity is higher, the calculated Darcy velocities are intermediate to the range determined at Äspö (see Figure 3.3 and Table 3.2). The absence of very high flux values for the Finnsjön site is largely due to the fact that, according to the geological structural model (SKB, 1992) that has been assumed to be correct for this analysis, there are no fracture zones close to the repository. Hence flow and transport are assumed to pass through large thicknesses of the rock mass, in both calculation cases. Moreover, in the analysis for Finnsjön, the range of evaluated head differences has been limited to using the measured head below Zone 2 for the vertical transport case, and the regional gradient for the lateral transport case. Higher velocities would clearly be calculated if the same range of gradients and the same proximity of fracture zones were applied as at Äspö.

It may be noted that the Darcy velocity predicted from these simple calculations for the lateral flow case (Finnsjön Case 1) is in agreement with the geometric mean of all realizations, in the stochastic-continuum analysis of the SKB-91 repository (Figure 9-9, SKB, 1992).

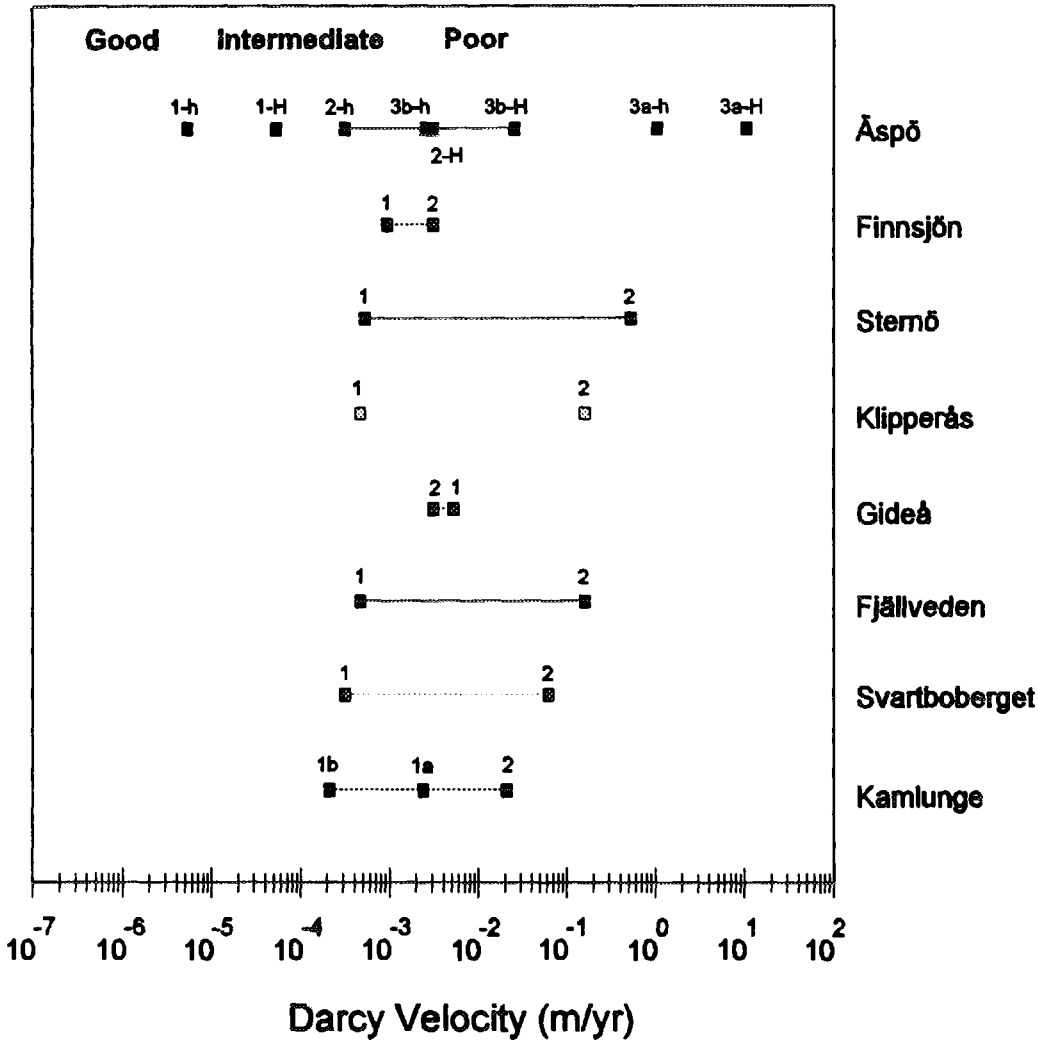

DWG0141a

Figure 3.3. Comparison of predicted ranges of Darcy velocity among the eight study sites. The labels "Good," "Intermediate," and "Poor" indicate the approximate classification according to Darcy velocity, as defined in Project-90 (SKI, 1991). Labels on individual data points indicate the calculation cases, as defined in the preceding text. For the Äspö cases, the suffix "-h" indicates cases with lower (local) excess head, and the suffix "-H" indicates cases with higher (regional) excess head. Cases 1 and 3a for Äspö represent special cases that were evaluated for Äspö but do not have direct equivalents for the other sites.

Table 3.2. Summary of results of simple hydrological analysis

	Case	Darcy velocity q (m/yr)	Equivalent to Project-90 Near-field	Far-field	Hydraulic cond. K (m/s)	Transport distance (m)	Hydraulic head gradient
Äspö	1	5.4×10^{-5}	normal/good	normal/good	1.0×10^{-10}	600	1.7×10^{-2}
		5.4×10^{-6}			1.0×10^{-10}	600	1.7×10^{-3}
	2	3.2×10^{-3}	poor/normal	non-existent	1.0×10^{-10}	10	1.0×10^{0}
		3.2×10^{-4}			1.0×10^{-10}	10	1.0×10^{-1}
	3a	1.05×10^{1}	worse than	worse than	2.0×10^{-5}	600	1.7×10^{-2}
		1.05×10^{0}	poor	poor	2.0×10^{-5}	600	1.7×10^{-3}
	3b	2.6×10^{-2}	poor/normal	poor/normal	5.0×10^{-7}	600	1.7×10^{-2}
		2.6×10^{-3}			5.0×10^{-7}	600	1.7×10^{-3}
Finnsjön	1	9.5×10^{-4}	poor/normal	poor/normal	1.0×10^{-8}	5000	3.0×10^{-3}
	2	3.2×10^{-3}	poor/normal	poor/normal	1.0×10^{-8}	100	1.0×10^{-2}

Comparison of Äspö with other sites

The calculated Darcy velocities for all of the study sites, considered together, vary over more than four orders of magnitude (Figure 3.3). In terms of the Project-90 classification (SKI, 1991), most of the calculations indicate intermediate to poor Darcy-velocity conditions.

For most sites, the difference between the best-case and worst-case Darcy velocity is two to three orders of magnitude. Notable exceptions are the cases of Finnsjön and Gideå, for which the predicted ranges are much narrower. In the case of Finnsjön, the narrow range of Darcy velocity is largely due to the somewhat optimistic assumption, based upon the SKB-91 interpretation, that there is at least 100 m of good-quality rock mass between the repository and the nearest highly conductive structure. If smaller-scale fracture zones exist within the rock mass at this site, as suggested by interpretations of borehole fracture and radar data (see *e.g.* Geier *et al.*, 1992), this distance would be substantially reduced. For a less optimistic distance of 20 m, the maximum Darcy velocity for Finnsjön would increase to 1.6×10^{-2} m/yr.

In the case of Gideå, the narrow range is due to the fact that only discharge through the rock mass has been considered, and no evaluation has been made of the effects of variability within the rock mass, whereas for the other sites heterogeneity in the form of higher-conductivity fracture zones has been taken into account. As noted in Section 3.5.1, the conductivity of the rock mass at Gideå is sufficiently variable that fracture zones are not hydrologically distinguished.

The Äspö cases equivalent to the cases chosen for most of the other sites (2-h, 3b-h, and 3b-H) give a Darcy velocity range similar to those sites, as shown in Figure 3.3. The range between the best and worst cases at Äspö (Cases 1 and 3a, respectively) is five orders of magnitude. This is due primarily to the hydraulic conductivity which differs by five orders of magnitude between Äspö fracture zones and rock mass. Although the other sites may contain fracture zones with conductivity approaching the highest values at Äspö (*e.g.* Zone 2 at Finnsjön; see Ahlbom *et al.*, 1992c), cases with a direct connection to such a structure have been considered only for Äspö (For Sternö a direct connection to a lower-conductivity fracture zone is considered).

Thus, based on these few example calculations, the availability of significantly more field

data at Äspö, than at the other sites, does not necessarily lead to a more narrow range of predicted Darcy velocities. Rather, the more detailed characterization of Äspö allows consideration of more cases, resulting in wider ranges of interpreted variability in hydraulic conductivity for potential radionuclide release pathways. This in turn has led to a wider predicted range of Darcy velocities. Thus existence of more data may lead to a need to consider potential pathways with a wider range of properties than might be judged from less data.

4 Simple predictions of far-field transport

4.1 General effects of pore geometry

The interrelationships among groundwater flux, advective velocity, and wetted surface area encountered by radionuclides, as they migrate toward the biosphere, are investigated by considering a variety of simple, idealized models for the pore geometry within transmissive features in the rock. These models, as described in Section 2.3.3, are used due to the shortage of field data which could provide empirical constraints on these relationships. Results are obtained for the flow wetted surface, the F ratio, and porosity. The ratio of flow wetted surface area to pore volume controls the partitioning of radionuclides between mobile and sorbed states, and hence governs retardation due to sorption. The porosity gives the ratio between groundwater flux (Darcy velocity) and the advective velocity u, which controls the arrival of nonsorbing species.

4.1.1 Effects of alternative assumptions

Figure 4.1 illustrates the importance of assumptions concerning pore geometry, in terms of the F ratio (which is a measure of the reactive transport properties) and the porosity for each model. The F-ratio values in this figure are normalized with respect to the head gradient $\Delta h/L$ and transport distance L. Model A is a simple planar fracture, with an aperture b corresponding to a transmissivity of 10^{-6} m^2/s (representative of typical fracture zones), in a 10 m thickness of rock (a typical fracture-zone thickness). The parameters of the other illustrative models are chosen to give the same net flux as Model A, for a given head gradient.

Model B, the tubular-channel model, is an extreme case which gives the lowest values of both F and porosity. Model C, which consists of n equal-aperture, planar fractures, gives increased values of F and porosity depending on the number n. Model D and E are stepped-fracture models. In Model D, flow is parallel to the steps ("with the grain") so that aperture is constant along stream lines. In Model E, flow is perpendicular to the steps ("across the

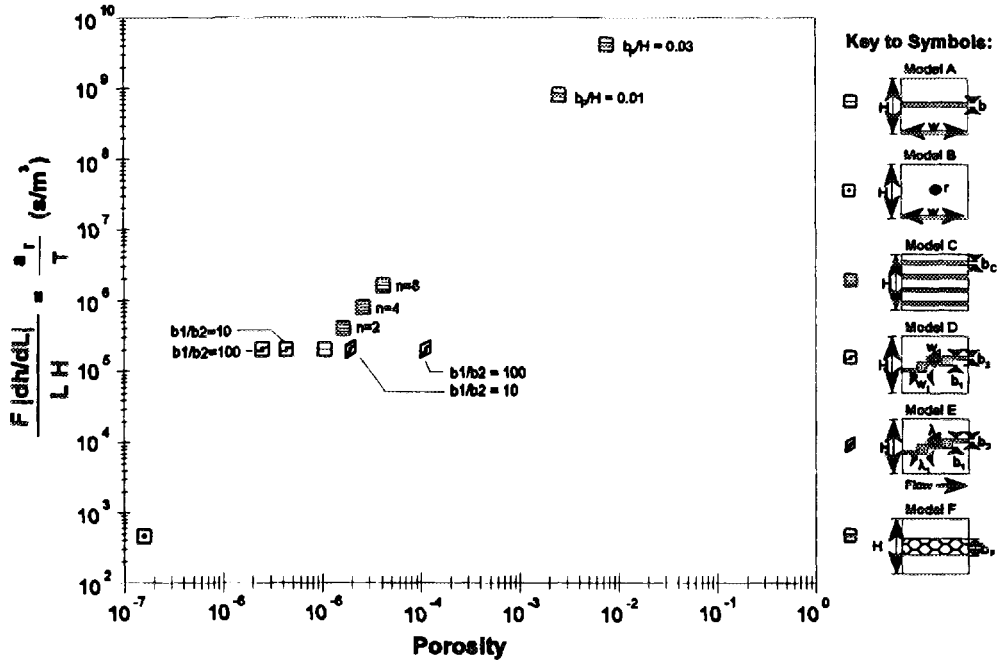

Figure 4.1. Effect of alternative assumptions concerning the structure of pore space on effective values of the F ratio and porosity. Comparisons for various simple models of pore geometry: (a) a single, parallel-plate fracture, (b) a cylindrical tube or channel, (c) n equal-aperture, parallel-plate fractures, (d) stepped fracture with aperture varying perpendicular to the direction of flow, (e) stepped fracture with aperture varying along the direction of flow, and (f) a parallel-plate fracture packed with uniform, spherical particles. For all models the thickness H = 10 m and the width w = 1 m. The aperture b in Model A corresponds to a transmissivity of 10^{-6} m^2/s. The parameters of all other models are chosen to give the same net flux as Model A, for a given gradient.

grain") so that aperture varies along stream lines. For aperture values in the range of interest, the values of specific surface a_w in Models D and E are nearly equal to that for Model A, and hence F does not vary appreciably. However, a wide range of porosity values can be produced depending on the aperture ratio $\beta = b_1/b_2$, and whether the aperture varies parallel to or perpendicular to the direction of flow. Model F, representing a crushed zone, gives the highest values of both F and porosity.

Although the models in Figure 4.1 are most readily interpreted in terms of individual, discrete fractures or fracture zones, they also provide simple models for the pore structure of the rock mass. If the rock mass is considered to consist of identical, equally spaced

features from one of the models A-F, the effective rock mass conductivity is equal to the transmissivity for a single such feature, divided by the spacing H between fractures or fracture zones.

4.1.2 Constraints on combinations of groundwater flux and pore geometry

Although a very wide range of transmissivity (and hence groundwater flux) values can be accommodated with any of the pore-geometry models A-F, by a suitable choice of parameters, not all combinations of transmissivity values with pore-geometry models are plausible. By taking into account limits on the observed ranges of transmissivity and porosity, for different types of transport pathways, uncertainty in the predicted F ratio can be reduced. The following observations have been taken into account for this purpose.

A first basic constraint is provided by field measurements of porosity. For fracture zones, relevant estimates are available from analyses of a radially converging tracer test at Finnsjön (Gustafsson and Nordqvist, 1993), which gave θ estimates in the range from 0.001 to 0.05, and from 0.01 to 0.1, within different subzones of a major fracture zone. Allowing for the existence of less porous fracture zones which are barely distinguished from the rock mass, a range of 10^{-4} to 10^{-1} for fracture-zone porosity has been assumed in the present analysis.

For transport through the rock mass, relevant estimates of porosity are available from the Stripa 3-D migration experiment (Abelin *et al.*, 1987), which gave estimates of $\theta = 2\text{x}10^{-5}$ to $1.5\text{x}10^{-4}$. Allowing for the possibility of less porous portions of the rock mass, which might be difficult to characterize in a migration experiment, a range of 10^{-6} to 10^{-4} has been assumed for rock-mass porosity.

A second basic constraint is provided by the ranges of transmissivity that have been measured in the field. For a single fracture, the realistic range of transmissivity should correspond to the measured values from small-scale packer tests in boreholes. Typically such measurements range from below the resolution of the packer-testing system to as high as 10^{-4} m^2/s. Although values above 10^{-6} m^2/s often correspond to crushed zones rather than single discrete fractures, in order to be conservative, it is assumed here that single-fracture transmissivity may fall anywhere in this range (*i.e.* $T < 10^{-4}$ m^2/s, with no lower bound). This constraint is applied to the single-fracture models of pore geometry, Models A, D, and E.

For the multiple planar-fracture model (Model C), the maximum transmissivity value should not be much greater than that for a single fracture. This is because the transmissivities of individual fractures are typically observed to follow a lognormal distribution, with the vast majority of the fractures having T values that are orders of magnitude lower than the most transmissive fractures. Therefore it is unlikely that any cluster of fractures will contain more than a few fractures of extremely high T. Since the maximum value for single-fracture transmissivity of 10^{-4} m^2/s is already quite conservative, it can safely be assumed that $T < 10^{-3}$ m^2/s.

When the constraints on porosity are applied to the tubular-channel model (Model B), it is found that this model cannot be considered as a representative for either the rock mass or major fracture zones at Äspö. In order to produce transmissivities and hydraulic conductivities consistent with the ranges being evaluated for Äspö, the porosity is in general found to be less than 10^{-4} for the fracture-zone cases, and less than 10^{-6} for the rock-mass cases, regardless of what value is assumed for the channel spacing w. Thus it is not reasonable to expect a fracture zone, or a large region of the rock mass, to conduct water solely through conduits of this type. Although such channels could conceivably occur in conjunction with other types of conductive elements (*e.g.* simple fractures), and thereby yield reasonable net porosities for the rock mass or a fracture zone, the additional wetted surface area provided by the other types of elements would result in higher, and thus less extreme F ratios.

This does not exclude the possibility that isolated conduits similar to Model B might exist within the rock mass or a fracture zone. This model is considered in this simple evaluation as a limiting case, which gives an absolute lower value on the F ratio. Although such extreme channels cannot sensibly be related to effective, bulk properties of the rock (hydraulic conductivity, porosity, *etc.*), the effect of a single such channel on far-field performance can be analyzed by calculating the F ratio, according to the formula derived in Appendix A.2. The consequences of extreme tubular channels, such as are represented by Model B, are addressed in Section 4.2.4.

The plausible range of properties for the crushed-zone model (Model F) is difficult to assess without site-specific analyses to correlate flow and transmissivity estimates with crushed

zones of various geometries. However, experience suggests that crushed zones tend to coincide with high transmissivity values and active flow paths (see *e.g.* the qualitative analysis of Äspö data for SITE-94, by Voss *et al.*, 1996). In the present analysis, this model is considered to apply for the transmissivity range 10^{-8} m^2/s < T < 10^{-3} m^2/s.

Lower-transmissivity crushed zones might well exist, but would require relatively fine-grained filling material. As the grain size becomes small relative to the penetration depth for matrix diffusion and sorption within microfissures, the actual retardation capacity will become less than indicated by the calculated value of the F ratio. For example, for a 15 cm thick crushed zone with $T < 10^{-8}$, the corresponding grain size required by Model F is $r_f < 1$ mm. In the far-field consequence calculations for SITE-94 using CRYSTAL, penetration depths of δ = 5 to 10 cm have been used to model surface sorption (SKI, 1996). Obviously the retardation capacity that is predicted by CRYSTAL, for a transport pathway composed of ordinary fractures separated by relatively thick rock slabs, may not be fully realized for a transport pathway described by Model F, when $r_f \ll \delta$, even if the F ratios are identical for the two cases. Therefore, although extremely high (favorable) values of the F ratio could be produced by combining Model F with lower values of T, analyses of such combinations are not presented here.

4.2 Predictions of radionuclide transport at the Äspö site

The simple evaluation of radionuclide transport at the Äspö site consists of an evaluation of all plausible combinations of the simple hydrologic models (Chapter 3) with the pore-geometry models as described above. Incompatible combinations are excluded as discussed in Section 4.1.2.

The evaluations are in terms of the F ratio, which for a given Peclet number *Pe* can be related directly to far-field geosphere performance (see Figure 2.1). Constraints on *Pe* are not readily derived, due to the fact that this depends largely on dispersion caused by irregularities in the flow field, which are not represented in the simple models. However, according to the SITE-94 scoping calculations with CRYSTAL (SKI, 1996) for the case of reactive species, *Pe* is much less important than *F* in terms of far-field geosphere performance .

Values of the F ratio are calculated using the formulae in Table 2.1, results of the groundwater flow calculations in Chapter 3, and the following parameters for the specific models:

For the simple planar fracture (Model A), the hydraulic aperture b is calculated from the transmissivity value T for the specific case, using the cubic-law relationship:

$$b = \sqrt[3]{T/c} \tag{28}$$

where c is a physical constant as defined in Section 2.4.

For the tubular channel model (Model B), a reasonable value for the spacing w between channels is suggested by the results of Palmqvist and Lindström (1991), who found a typical spacing of 2 to 4 m between "point inflow" indications in two tunnels in granitic rock. Higher values of w are more conservative since they produce more concentrated flow and lower F ratios, and hence reduced retardation of radionuclides. In this study, a wide range of channel spacings were considered (w = 0.1 to 10.0 m). In all cases it is found that the resulting porosity θ is lower than the admissible ranges, as discussed above.

For the multiple planar-fracture model (Model C), the number of fractures in each fracture swarm is taken as $n_C = 20$, which can be viewed as a very high value. Higher concentrations of fractures would tend to resemble crushed zones, which would be better represented by Model F. High values of n_C produce a greater contrast between this model and the simple planar fracture.

For the stepped-fracture models (Models D and E), the following parameter values are used: $\beta = 100$, $w = l = 1$ m, and $\omega = \lambda = 0.1$. High values of β and low values of ω and λ imply relatively strong segregation between high-aperture and low-aperture segments of the fracture, and hence greater contrast with the simple, planar-fracture model. The value of β used here is slightly high relative to the maximum ratios of "visual" aperture b_v to hydraulic aperture b that were measured by Abelin *et al.* (1990), in single fractures at Stripa. The values of b_v/b measured by Abelin *et al.* ranged from about 20 to 62, and are high relative to comparable data from other single-fracture experiments (see Geier *et al.*, 1992). The values of ω and λ correspond to the fraction of the fractures' surface area that carries most of the water, which according to Rasmuson and Neretnieks (1986) ranges from 5 to 20% for Swedish bedrock. The value of 1 m for w and l corresponds to the separation between channels that was used by Rasmuson and Neretnieks; variation of these parameters within the range 0.5 m to 5 m are found to not strongly affect the results given below.

For the stepped fracture flowing with the grain (Model D), the threshold value $b_{\mu m}$ below which the lesser-aperture portions of a fracture are considered to be accessible only by diffusion is arbitrarily set to 1 μm. For all cases presented below, the lesser-aperture segments of the fracture are of aperture less than this value, and hence the surface area of these segments is treated as being not directly accessible to radionuclides passing through the active channels.

For Model F, the crushed-zone width is taken as $b_F = 15$ cm, which is a typical crushed-zone width seen in the core data from Äspö. The porosity within the crushed zone is taken as $\phi = 1 - \pi/3\sqrt{2} = 0.26$, which represents hexagonally-packed, uniformly sized, spherical grains, and is the lowest possible value for this simple model. Higher values of ϕ lead to higher values of F and more effective retardation, and hence 0.26 may be viewed as a conservative value for ϕ, within the constraints of this model. Lower values of ϕ can in fact result from

variably sized grains (*e.g.*, porosities as low as 0.10 in synthetic fault gouges were measured by Marone and Scholz, 1989). However, consideration of variably sized grains would entail more complicated relationships among the basic hydrologic parameters, and would thus depart from the aims of this simple evaluation.

4.2.1 Case 1: Transport upward through the rock mass

For the hydrologic Case 1, as defined in Section 3.1.4, the discharge is by upward flow via the rock mass. To evaluate this case, the rock mass is considered to consist of uniformly spaced, transmissive features (single fractures, channeled fracture planes, or fracture swarms) corresponding to Models A through E (fractures, channels, *etc.*). The spacing between these features is taken to be $H = 5$ m for all cases. The transmissivity of each feature is calculated as $T = K/H$, where K is the rock mass conductivity.

The crushed-zone model (Model F) is not applied to this calculation case, because (1) such a pervasive population of crushed zones as this is not realistic, (2) the transmissivity range for individual features is well below that for which this model is considered to apply, and (3) crushed zones are more usually associated with fracture zones rather than with the rock mass. The tubular-channel model (Model B) is not applied to this calculation case, because it gives unreasonably low bulk porosity values for the rock mass as discussed in Section 4.1.2.

Figure 4.2a shows the values of F calculated for each of the pore-geometry models, for rock mass conductivities ranging from $K = 10^{-11}$ m/s to 10^{-9} m/s, for head differences $\Delta h = 1$ m and 10 m. The lowest F are produced by Model D (stepped fractures flowing with the grain). The highest F are produced by Model C (multiple planar fractures). However, the differences among Models A, C, and E are comparable in magnitude to the effect of an order-of-magnitude shift in rock-mass K.

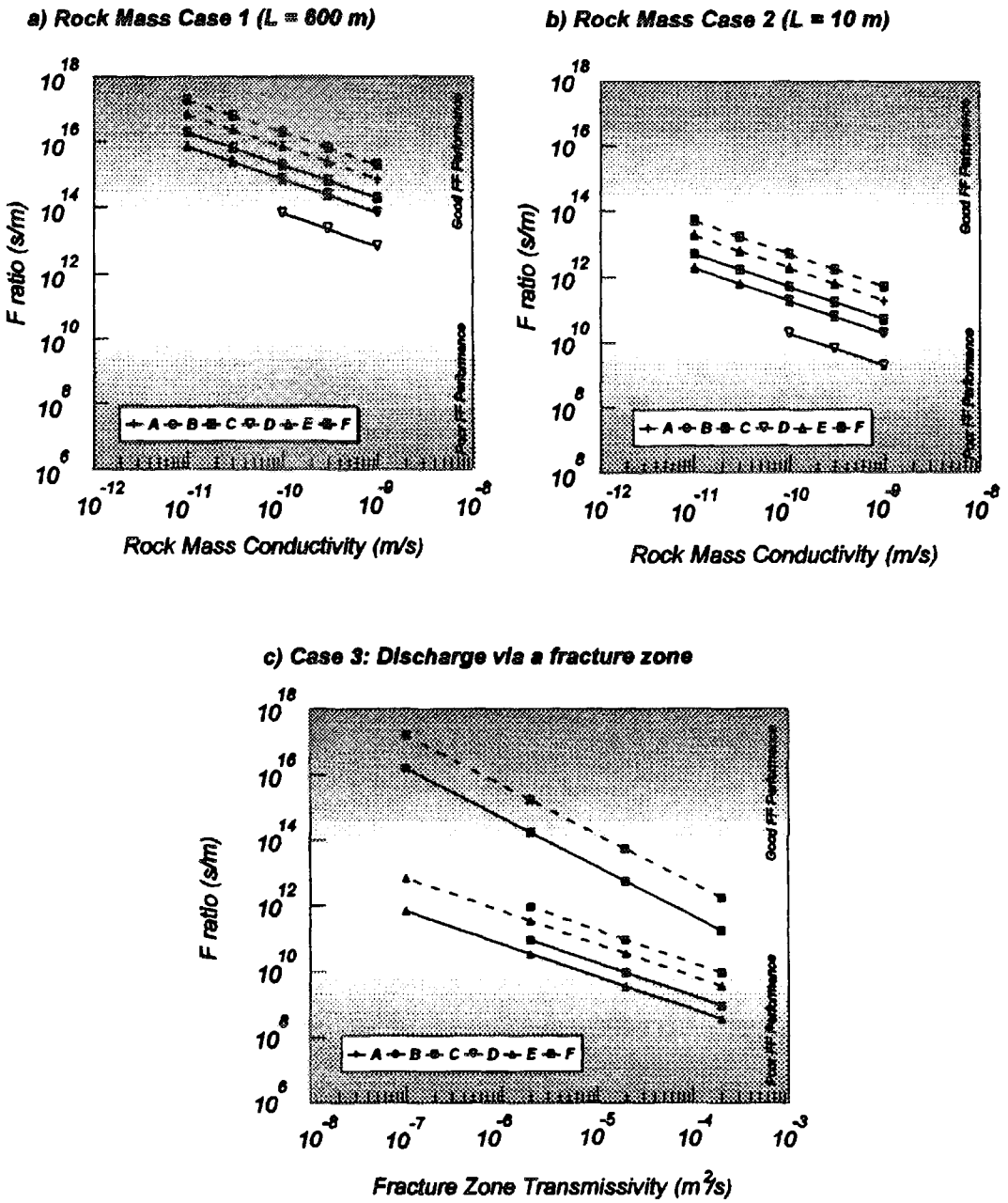

Figure 4.2. Simple evaluation of transport parameters for pore-geometry models A through F, including a) Case 1: vertical discharge via the rock mass, b) Case 2: discharge to a major fracture zone via a short path through the rock mass, and c) Case 3: discharge via a fracture zone. Solid lines pertain to the case of the lower hydraulic head difference, and dashed lines pertain to the case of higher head difference, for each case, as set forth in Section 3.1. Approximate ranges of "good" and "poor" far-field geosphere performance, based on the consequence calculations described in Section 2.3, are indicated with shading.

4.2.2 Case 2: Transport through the rock mass to a discharging fracture zone

For the hydrologic Case 2, as defined in Section 3.1.4, the discharge is via a short (10 m) thickness of the rock mass, before reaching a discharging fracture zone which is assumed to give no significant retardation. This case was evaluated using the same assumptions for the rock mass as above, but with a transport distance of 10 m rather than 600 m.

Figure 4.2b shows the values of F calculated for each of the pore-geometry models, for rock mass conductivities ranging from $K = 10^{-11}$ m/s to 10^{-9} m/s, for head differences $\Delta h = 1$ m and 10 m. As in Case 1, the lowest values of F are produced by Model D, while the highest values are produced by Model C. The differences among Models A, C, and E are again comparable to the effect of an order-of-magnitude shift in rock-mass K.

4.2.3 Case 3: Transport through a discharging fracture zone

For the hydrologic Case 3, as defined in Section 3.1.4, the discharge is via a discharging fracture zone which connects directly to the radionuclide source via the disturbed-rock zone (DRZ). The DRZ is assumed to have the same hydraulic properties as the fracture zone. This case is evaluated by considering a range of transmissivity values for the fracture zone, and calculating the corresponding F ratios for each of the pore-geometry models.

Figure 4.2c shows the values of F calculated for each of the pore-geometry models, for fracture-zone transmissivities ranging from $T = 10^{-7}$ m^2/s to $2\text{x}10^{-4}$ m^2/s, for head differences $\Delta h = 1$ m and 10 m. Imposition of the minimum porosity constraints, as discussed in Section 4.1.2, lead to the exclusion of the tubular-channel model (Model B) and, over much of the transmissivity range, the single-fracture models A and D. Model E (stepped fracture flowing across the grain), which is also a single-fracture model, yields higher porosities for a given transmissivity and is therefore applied over most of the transmissivity range. Model C, the multiple, planar-fracture model, also produces reasonable value of porosity over part of this transmissivity range.

The lowest F ratios are produced by the single-fracture models (Models A and E), for the transmissivity ranges where they apply. The differences between the F ratios calculated from these are not significant for the purpose of this simple evaluation. The highest F ratios are

produced by the crushed-zone model (Model F), which gives a high ratio of surface area to transmissivity. The differences among Models A, C, and E are generally comparable to the effect of an order-of-magnitude shift in rock-mass K.

4.2.4 Extreme channeling case

As discussed in Section 4.1.2, the extreme channels represented by Model B cannot be viewed as fully accounting for the effective, bulk properties of the rock, such as hydraulic conductivity and porosity. However, the possibility cannot be excluded that isolated conduits similar to the tubular channels in Model B, with a high **conductance** C_B (defined as the product of hydraulic conductivity times cross-sectional area), might exist within a repository in granitic rock such as at Äspö.

Due to the small cross-sectional area, the probability of penetrating such a channel with a site-characterization borehole is very small (Moreno and Neretnieks, 1991). Detection with geophysical methods such as borehole radar is also unlikely, due to the essentially 1-D geometry of such channels. On the other hand, the same characteristics that would make a channel difficult to detect would also lead to a low probability that one connects with a radioactive-waste deposition hole. This low probability should be taken into account in considering the calculations given below.

Due to the low probability of detection, it is difficult to estimate the maximum conductance C_B for a channel that might exist at Äspö, similar to those in Model B. A value of 2×10^{-7} m^3/s corresponds to the highest value of C_B that was estimated, for a conduit exhibiting linear (1-D) flow characteristics, by Generalized Radial Flow analysis of hydrologic packer test data from Äspö (Geier *et al.*, 1996). There is no direct evidence of higher-conductance channels at Äspö, but as noted, the probability of intersecting such a channel with one of the boreholes at Äspö is very small. However, rough indications of the possible frequency of higher-conductance channels are available from a field study by Palmqvist and Lindström (1991), who mapped instances of point inflow along two tunnels, the Saltsjö tunnel in Stockholm, and the Kymmen tunnel in Värmland.

In the Saltsjö tunnel, which lies mainly in granite, at a depth of 50 to 60 m, the highest estimated inflow rates in a 720 m length of tunnel were for two point inflows, in the range

1.5 to 6.5 liters per minute. Based upon an assumed hydraulic gradient of 5 m head per meter at the tunnel wall, the conductances of the observed conduits are in the range $5x10^{-6}$ to $2x10^{-5}$ m^3/s. In the Kymmen tunnel, which lies 50 - 200 m deep in bedrock consisting of leptite, granite gneiss, and amphibolite, six point inflows in the same range (1.5 to 6.5 liters/min), and four with even higher flowrates (> 6.5 liters/min) were observed within a 4500 m length of tunnel. However, the Kymmen data are less relevant for estimating the likelihood of high-conductance channels at the Äspö site, due to the contrast in lithology. In the Saltsjö mapping, roughly one channel with $C_B = 2x10^{-5}$ m^3/s was found per 360 m of tunnel.

Table 4.1 gives F ratios for Model B as a function of channel conductance and hydraulic driving forces. Values of C_B range from $1x10^{-9}$ m^3/s to $2x10^{-5}$ m^3/s. Hydraulic head differences, for a 600 m flow path length, are 1 m and 10 m, as for the other Äspö calculation cases. The far-field geosphere performance indicated by the calculated F ratios ranges from intermediate bordering on poor, for the lowest-C_B channels, to very poor, for the highest-C_B channels., according to the criteria for F ratio as set forth in Section 2.3.

Table 4.1. Values of F ratio for Model B, a cylindrical channel model. The transport distance L = 600 m in all cases. For each value of channel conductance, F ratios are calculated for each of the levels of hydraulic driving force (Δh) that are considered in the simple evaluation of groundwater flow for Äspö.

Conductance C_B (m^3/s)	Channel Radius r_B (mm)	Head Difference Δh (m)	F ratio F_B (s/m)
$1.0x10^{-9}$	0.13	1	$2.9x10^{11}$
		10	$2.9x10^{10}$
$1.0x10^{-8}$	0.23	1	$5.1x10^{10}$
		10	$5.1x10^{9}$
$2.0x10^{-7}$	0.48	1	$5.4x10^{9}$
		10	$5.4x10^{8}$
$2.0x10^{-6}$	0.85	1	$9.6x10^{8}$
		10	$9.6x10^{7}$
$2.0x10^{-5}$	1.50	1	$1.7x10^{8}$
		10	$1.7x10^{7}$

4.2.5 Evaluation of results

From the results for Case 1 (transport through the rock mass to the surface) it is evident that, when release to the biosphere occurs solely via vertical discharge through the entire thickness of rock mass, the F ratio is high ($F > 7 \times 10^{12}$ s/m) for the applicable pore-geometry models. Even for a model that includes channeling within fracture planes (Model D), the F ratio is at least in the range corresponding to intermediate far-field performance, as defined in Section 2.3. Thus, if a repository can be designed and built in such a way that discharge via major fracture zones or extreme channels is avoided, far-field performance should be good. It should be noted that this observation applies specifically to the case where the rock mass is macroscopically homogeneous in conductivity (*i.e.*, the spatial organization of high-conductivity elements in the rock mass is essentially random, rather than being organized in a network that exhibits hydrogeological scale effects up to the scale of the rock-mass thickness).

For Case 2 (transport through the rock mass to a discharging fracture zone), the F ratios range from high (10^{14} s/m) to medium or even low (10^{9} s/m), depending upon the hydraulic driving forces and the rock mass *K*. Poor far-field performance can result either from channelization of the flow path (as exemplified by Model D) or from a combination of high conductivity and high hydraulic gradient. Thus for this type of discharge path, uncertainties in hydraulic gradient and conductivity are of an importance comparable to uncertainties in pore geometry (degree of channelization) in determining far-field performance.

For Case 3 (transport through a fracture zone to the surface), pore geometry is a major factor affecting far-field performance, for moderately transmissive fracture zones in the range 10^{-8} $m^2/s \leq T \leq 10^{-5}$ m^2/s. Fracture zones that behave like Model F (crushed-zone model) give markedly higher F ratios and hence significantly better far-field performance than the models with more distinct fractures. However, for highly transmissive fracture zones, even Model F gives intermediate-to-poor far-field performance.

Very low values of the F ratio ($1x10^9$ s/m or less) can result from the presence of extreme flow channels, as represented by Model B. For such low values of the F ratio, far-field retardation will be negligible (SKI, 1996). Thus the presence or absence of extreme channels (and their spatial intensity, if present) is a crucial factor affecting far-field performance.

5 Discussion

5.1 Comparison among sites in terms of hydrogeology

The estimated Darcy velocity range is from 10^{-4} to 10^{-2} m/yr for typical cases, at all sites, and up to 10^{0} m/yr for extreme cases. The former range is equivalent to "intermediate to poor" Darcy velocity conditions, as defined in SKI Project-90 (SKI, 1991), and the latter value is extremely poor.

Although much more detailed data are available for Äspö, the range of Darcy velocity is not more narrowly defined for Äspö than for the other sites. In fact, the range of possible velocities is in general somewhat wider than for the other sites. This may largely be due to the consideration of more extreme cases for Äspö such as flow through only low-conductivity rock mass and flow only through a highly permeable fracture zone (and disturbed-rock zone). While Äspö has been interpreted as containing a higher intensity of conductive structures than the other sites, it may be speculated that this is simply a consequence of the more intensive site-characterization program at Äspö.

Main factors for prediction of hydrogeology at the sites

The most important parameter controlling net Darcy velocity is **hydraulic conductivity**. However, the determination of an effective hydraulic conductivity is associated with great uncertainty. Data within each site exhibit a tremendous range of K (usually 5 orders of magnitude). At some sites, fracture zones are indistinguishable from the rock mass in terms of conductivity. There is also a similarly large variation of K within defined fracture zones, implying that flow uniformity, and possibly continuity, may not always exist in such zones.

The existing data give little or no information regarding how conductive elements within the rock mass and fracture zones are connected in space. Such information is crucial to the precise prediction of site hydrogeology.

The largest range of possible **hydraulic gradients** affects Darcy velocity only over one order of magnitude, except where local topography variation is great as at Kamlunge.

The assumption of **direction of flow** (upward or downward) through the repository does not affect the estimation of flux. However, downward or lateral flux increases travel distance and hence will usually increase the wetted surface available to retardation processes, over that which is expected for the case when flux is directed upward.

5.2 Far-field performance at Äspö

The predicted range of F ratio values for Äspö is roughly from 10^8 to 10^{16} s/m. Based on scoping calculations carried out within SITE-94 using CRYSTAL (SKI, 1996), these values of the F ratio can be related to performance of the far field as a barrier to radionuclide migration (see Figure 2.1). Values below 10^{11} s/m, corresponding to poor to very poor performance (negligible far-field barrier function), in general represent somewhat pessimistic assumptions concerning the hydrological connections (*e.g.* direct connection to a fracture zone), or the pore geometry (*e.g.* extreme channels), or both. Even for the less pessimistic cases, the predicted F ratios still span a very wide range, from marginally poor to very good far-field performance.

It should be noted that, in these calculations of F ratio, it has been assumed that all surface area within a conduit is available for sorption and matrix diffusion, and that the properties of the surface area are spatially uniform with respect to these processes. In reality, these processes are affected by additional factors such as fracture mineralogy and the type of pore structure within fracture minerals (*i.e.* coatings or infillings), which have not been considered.

The key factors affecting the F ratio predictions are the wide range of possible Darcy velocities and high uncertainty regarding the relationship between Darcy velocity and flow wetted surface area along potential transport paths (which is a practical consequence of high uncertainty regarding the detailed pore geometry within these paths). The wide range of possible Darcy velocities is mainly due to the wide bounds on effective hydraulic conductivity, as discussed in the previous section. This uncertainty probably cannot be significantly reduced without additional information about how conductive elements within the rock are connected in space, which is not available from the type of site-characterization data considered here (surface-based measurements). However, the uncertainty regarding interrelationships among parameters along transport paths could perhaps be reduced by generic and site-specific studies that directly address this issue.

Only a few combinations of hydraulic gradient, hydraulic conductivity, and pore-geometry models have been used in this analysis. A more detailed analysis could be made, but the

examples illustrate that the outcome may not necessarily provide more information than obtained here, given the sparse data available, and the lack of information on (1) connectivity among conductive structures, and (2) pore geometry within conductive structures (or, in practical terms, the consequences of connectivity and pore geometry for the relationships among effective parameters for groundwater flow and transport).

5.3 Comparison of simple evaluation and detailed models

The results of these simple, scoping calculations can be compared with the predictions of transport parameters, by more complex numerical models, within SITE-94, including:

- Discrete-feature (DF) model of Äspö (Geier, 1996),
- Stochastic continuum (SC) model of Äspö (Tsang, 1996),
- Detailed-scale, variable-aperture, fracture network (VAPFRAC) model (Nordqvist *et al.*, 1995).

These models in general make more intensive use of the available site-characterization data than does this simple evaluation. The DF model provides the most complete comparison with the present analysis, since it provided independent estimates of all relevant parameters. The SC model provided independent estimates of Darcy velocity and dispersion coefficients, but values of head gradients, porosity and specific wetted surface were required from other sources, in order to scale these estimates and calculate effective F ratios. The VAPFRAC model provided independent estimates of flow porosity and wetted surface, but the results are limited to the near-field rock mass, and velocity estimates are needed from other sources.

5.3.1 Comparison with the discrete-feature model

The discrete-feature (DF) model consists of a 3-D, deterministic representation of the fracture zones in the SITE-94 geological structural model of Äspö (Tirén *et al.*, 1996), combined with a stochastic, discrete-fracture-network representation of fractures within the hypothetical repository. The model integrates structural geological and hydrological data on scales ranging from semiregional (5 km) down to the detailed scale (1 m), with resolution of conductive elements increasing with proximity to the repository and to individual, radioactive-waste deposition holes within the repository. Hydraulically conductive elements within the domain of the model are represented as 2-D, transmissive planar features which connect to form a network in 3-D space.

The DF modelling for SITE-94 included a large number of variants to evaluate various conceptual and parametric uncertainties in the basic model. Uncertainty relating to the following aspects of the model were investigated: configuration and hydrological properties

of large-scale fracture zones, properties of the population of discrete fractures within the rock mass around the repository, boundary conditions on the semiregional scale, and properties of the disturbed-rock zone (DRZ) adjacent to repository shafts and tunnels.

Comparison in terms of Darcy velocity

The near-field Darcy velocities predicted by different variants of the DF model ranged from about 10^{-6} to 0.1 m/yr, which compares with a range of roughly 10^{-6} to 10 m/yr for the simple evaluation (Figure 5.1). If the most extreme simple-evaluation case (Case 3a, a direct connection to the biosphere via Fracture Zone NE-1) were excluded, the DF model would in fact predict a slightly greater range of Darcy velocity than does the simple evaluation. Moreover, it should be noted that a large majority of canister sites are predicted by the DF model to have Darcy velocities below the resolution of the model, and are not represented in this figure.

The wide range of Darcy velocities predicted by the DF model can be attributed to two possible factors: (1) the DF model includes a representation of stronger variability within the rock mass than does the simple evaluation, and (2) according to the DF model, strong connections to the biosphere, via a combination of high-transmissivity fractures and high-transmissivity fracture zones (similar to NE-1) are likely to occur at least occasionally. The latter would imply that Case 3a of this simple evaluation is not unduly pessimistic. The former points toward one potential weakness of the simple evaluation, namely that the consequences of structured heterogeneity for hydraulic conductivity within the rock mass (*i.e.*, a tendency for high-conductivity elements of the rock mass to occur in structures or networks, rather than purely randomly, leading to scale effects in hydrologic properties that persist on a large scale) are not directly addressed. In the present analysis, however, the simple evaluation cases (including fracture-zone cases) cover a wide enough range of possibilities that the simplifications with respect to the rock mass do not affect the overall range of predictions.

Comparison in terms of F ratio

When all DF model variants are lumped together as an expression of the total spatial variability plus (evaluated) uncertainty, the resulting, predicted range of F ratios is $2x10^{10}$ to $5x10^{14}$ s/m. Although this represents a reduction of several orders of magnitude, relative to the range predicted by the simple analysis (Figure 5.2), the predicted F ratios still span a very wide range, from marginally poor to very good far-field performance.

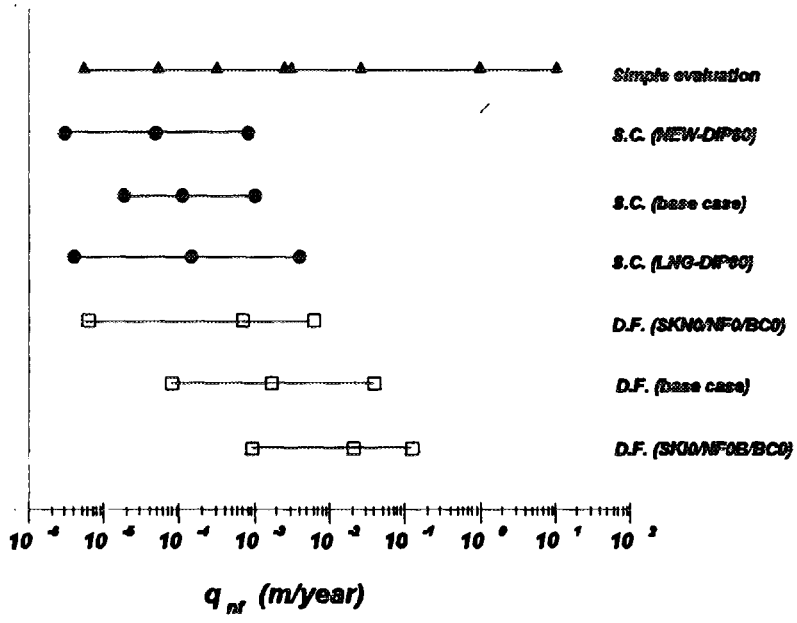

Figure 5.1. *Estimated ranges (spatial variability) of near-field Darcy velocity for the Simple evaluation and the two detailed hydrological site models. For the detailed site models the ranges of Darcy velocity correspond to the 10th percentile, the median and the 90th percentile of the estimated velocity distribution. The figure includes the base case and the variants that gave the lowest and the highest median Darcy velocity for the respective site model.*

5.3.2 Comparison with the stochastic-continuum model

In contrast to the DF model, the stochastic continuum (SC) model for SITE-94 (Tsang, 1996) treats the rock mass, including fracture zones, as a random, porous continuum that is everywhere hydraulically connected. Stochastic realizations of the 3-D hydraulic conductivity field are generated by a nonparametric, geostatistical technique, which results in anisotropic, long-range correlations among high-conductivity portions of the rock, along two sets of preferred planes which correspond to two of the main sets of fracture zones that are defined in the SITE-94 structural model (Tirén *et al.*, 1996). These stochastic realizations are conditional upon the measured hydraulic conductivities in boreholes. Uncertainty related to the hydraulic conductivity structure have been investigated by evaluating geostatistical models that give different correlation structures (*i.e.*, different tendencies for the hydraulic conductivities at any two given points to be correlated, depending upon the distance and direction of offset between the points).

The stochastic continuum model results (Tsang, 1996) were produced for an arbitrary head gradient, and hence site-specific estimates of the gradient were required to calculate Darcy velocities from the SC model results. However, this is not a major issue, as the uncertainty and variability in head gradients for Äspö are comparatively low. The range of calculated near-field Darcy velocities, based on the SC model results, was roughly 10^{-6} to 10^{-2} m/yr, which compares with a range of roughly 10^{-6} to 10 m/yr for this simple evaluation (Figure 5.2). Excluding the most pessimistic simple-evaluation case (Case 3a), the SC model and the simple evaluation yield similar ranges of Darcy velocity.

5.3.3 Comparison with the variable-aperture fracture network model

The variable-aperture, fracture-network (VAPFRAC) model for SITE-94 (Nordqvist *et al.*, 1995) is a 3-D, stochastic, discrete-fracture-network model in which the aperture varies lognormally within each fracture. The model was used in SITE-94 to produce estimates of specific flow wetted surface a_r. These estimates ranged from 0.1 to 10 m^2/m^3, with a median value of 2 - 3 m^2/m^3. For a flow porosity of $5x10^{-4}$, this corresponds to a median a_r of about $5x10^3$.

Figure 5.3 shows a graphical comparison between the VAPFRAC estimates of a_r and a_w and that of Models A-F, for a representative fracture transmissivity of 10^{-8} m^2/s, with all other parameters the same as in Figure 4.2a-c. Contours of equal porosity are shown as straight lines. In terms of a_w, the VAPFRAC results are close to those for Model E, which represents a stepped fracture with aperture variation along the direction of flow (series model). This result may be expected due to the similarity in the conceptual representation of fracture aperture variation in the two models. As indicated by the porosity contours, the differences between the VAPFRAC models and the simple single-fracture models (Models A, D, and E) in terms of a_r is primarily due to the different porosity of the models, which is due to a difference of approximately a factor of four in the assumed or effective fracture spacing (H).

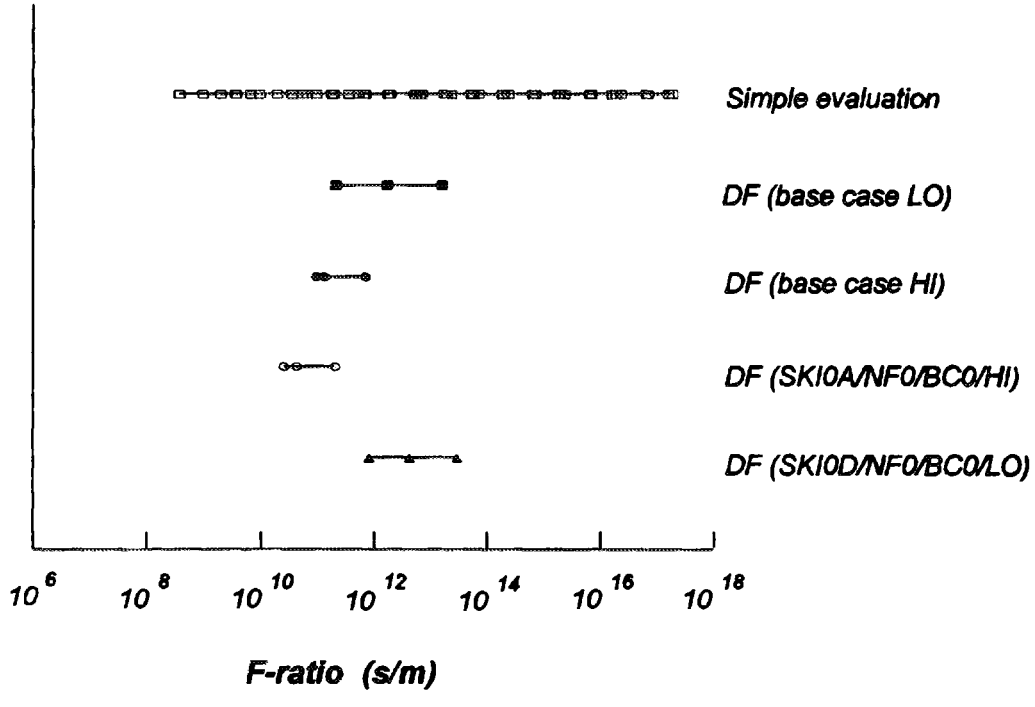

Figure 5.2. *Estimated ranges (spatial variability) of F ratio for the simple evaluation and the discrete-feature model. For the discrete-feature model the ranges of F ratio correspond to the 10th percentile, the median and the 90th percentile of the estimated F-ratio distribution. The figure includes the base case (results are shown for two different assumptions concerning the porosity of large-scale fracture zones) and for the for the discrete-feature model variants that gave the lowest and the highest median F ratio. These variants are defined by Geier (1996).*

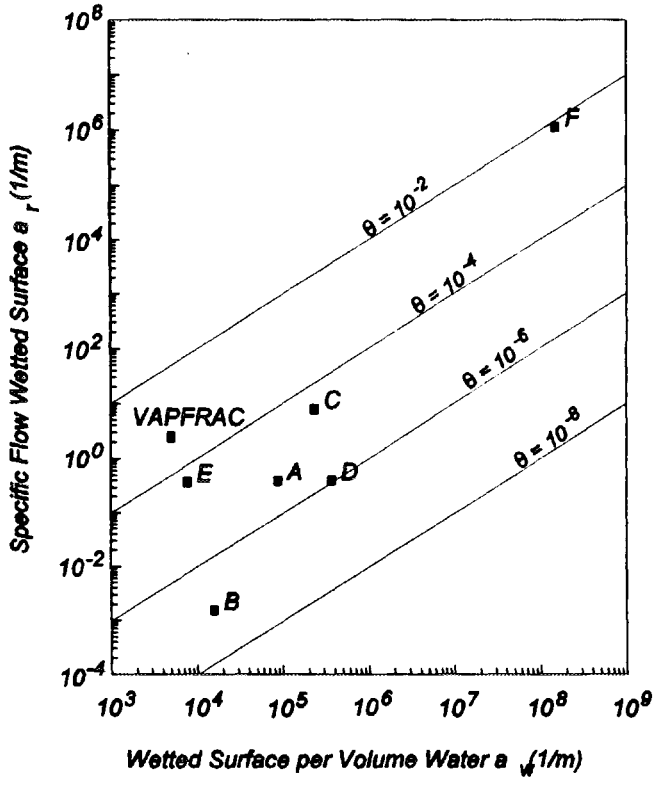

Figure 5.3. Comparison of simple pore-structure models with VAPFRAC results. Diagonal lines show contours of constant porosity.

5.3.4 Utility of detailed models vs. simple evaluation

The simple evaluation for Äspö yields predicted F ratios which span a very wide range, from very poor to very good far-field performance. The detailed models employed in SITE-94 reduce the breadth of the predicted range by a few orders of magnitude. However, the predicted F ratios from detailed models still span a very wide range, from marginally poor to very good far-field performance. Thus compared with what can be said from the simple evaluation, the detailed models do not markedly improve our ability to say, in absolute terms, whether the performance of the far-field system as a barrier is excellent, marginal, or poor. Thus the simple evaluation is a much more cost-effective means of evaluating site performance.

However, the detailed models do allow a distinction to be made between the effects of spatial variability, which is a natural property of the system, and uncertainty, which represents our imperfect understanding of the system. Although the overall ranges of Darcy velocity and F ratios predicted by the detailed models are nearly as large as those predicted by the simple evaluation, the detailed models show that a large portion of these ranges is attributable to spatial variability among the different canister sites. The median values of Darcy velocity predicted by different variants of the detailed models range over less than three orders of magnitude ($4x10^{-5}$ to $2x10^{-2}$ m/s).

The practical consequences of this distinction between spatial variability and uncertainty may not be fully evident at the repository siting stage, when the pattern of spatial variation at repository depth is still weakly characterized. In later stages of repository design, it might be possible to constrain the effects of spatial variability on overall performance, *e.g.* by accepting or rejecting particular canister sites based on detailed data from tunnels within a repository. However, at the siting stage, there is very substantial uncertainty regarding the properties of potential transport paths passing through any particular canister position within the repository. This uncertainty is reflected in the differences among stochastic realizations of the detailed models, in terms of the predicted flow and transport parameters for any given canister position.

At best, the detailed models give predictions of the proportion of canister deposition holes, within a site, that will be connected to transport paths with good, intermediate, or poor properties for radionuclide retention. Thus, whereas the simple evaluation delineates the possible range of performance, the detailed models may allow evaluation of the likelihood of a particular degree of performance. Such an evaluation must be predicated upon a specific set of conceptual assumptions and probability distributions for the parameters that define the models. The information thus obtained could be useful for evaluation of scenarios involving multiple canister failures, or for deciding whether a given site is sufficiently likely to contain enough "good" canister locations, to justify further investigation.

However, this advantage of the detailed models is diminished by the fact that many key aspects of uncertainty in the detailed models are not quantifiable. For example, the results in SITE-94 show that the surface-based data from Äspö can be reasonably well explained in terms of either of two different modelling concepts (stochastic-continuum and discrete-feature), which involve different assumptions regarding the structure of interconnection among conductive elements. To account for this type of conceptual uncertainty in a performance assessment, either some subjective evaluation must be introduced of the relative plausibility of the competing concepts, or the concepts must simply be considered side-by-side as alternative possibilities. Other types of uncertainty in the detailed models are also difficult to quantify, such as the choice of a particular form of geostatistical model in the stochastic continuum approach, and the choice of a particular structural model in the discrete-feature approach.

In summary, a simple evaluation is just as adequate as more detailed models for scoping the uncertainty in the performance of the geologic barrier at a site, given the type of data (measurements at the surface and in boreholes) that are available at the repository siting stage. The potential advantages of the more detailed models for performance assessment – their abilities to distinguish between spatial variability and uncertainty, and to yield probabilistic predictions based on propagation of quantified uncertainty in the data – are not fully realized at this stage. There are of course other grounds for using detailed models in a performance assessment, in particular the need to use multiple approaches to ensure that all relevant knowledge is brought to bear on the large uncertainties in the natural system. Moreover, these observations concerning the utility of detailed models pertain specifically

to the utility of these models for predicting the geologic barrier function in a performance assessment. The more complex models are indeed valuable for other purposes such as synthesis of data to provide feedback to the site-characterization process, testing of alternative repository designs, and modelling experiments which can lead to insights that are needed for the effective development of simple models.

5.4 Implications for site selection and safety analysis

Based on this simple evaluation of existing data, it is difficult to discriminate among the studied sites, in terms of estimated ranges of Darcy velocity. The only exceptions are the Finnsjön and Gideå sites, for both of which relatively narrow ranges of Darcy velocity are predicted. However, these narrow ranges are a result of the relatively limited range of cases that have been considered for the two sites. In the case of Finnsjön, the analysis assumes that at least 100 m of "good rock" exists between the repository and the nearest fracture zone, while for Gideå only discharge through the rock mass has been analyzed. A more thorough, simple evaluation of these sites, taking into account alternative geological interpretations, would likely produce Darcy velocity ranges comparable to the other sites.

Analyses of the Äspö data, using complex models, suggest that more intensive use of site data will not substantially reduce the predicted ranges of Darcy velocity. This appears to be a consequence of the typically high spatial variability in hydraulic conductivity, which in itself accounts for a major portion of the ranges of Darcy velocity.

The use of a mean hydraulic conductivity, as applied here, gives reasonable estimates of the net flux, but little direct information on transport of radionuclides along a real path from a repository to the surface. Such transport depends strongly on the detailed structure and connectivity of conductive elements in the rock.

Although the present, simple evaluation of transport parameters (F ratio) has been performed only for Äspö, it is clear that extending this analysis to all sites would lead to similar conclusions as were obtained with regard to Darcy velocity. That is, a wide range of F ratio, corresponding to far-field performance ranging from very poor to good, would be predicted for all of these sites. This can be expected due to the wide range of possible Darcy velocities, plus the high uncertainty regarding the detailed structure of porosity within transport paths, which in practical terms corresponds to high uncertainty regarding the relationship between Darcy velocity and flow wetted surface area.

Without new types of measurements at future sites, there will not be significantly more useful information available for performance assessment than is available now at Äspö or other sites. Given the type of data obtained, the predicted Darcy velocity at a site in the Swedish crystalline basement will likely be between 10^{-4} m/yr and 10^{-2} m/yr or higher, and the predicted F ratio will likely range from 10^{8} s/m to 10^{16} s/m, no matter which site is considered. The crucial information that is lacking concerns (1) the connectivity of different conductive elements, in the rock mass and in the fracture zones, and (2) the relationship between Darcy velocity and flow wetted surface area for different types of transport paths.

Given the wide estimated ranges of F ratio, in combination with the SITE-94 consequence calculations (SKI, 1996), it is not possible to confirm the effectiveness of the geologic barrier function for a repository in crystalline rock, based on the type of data available from surface-based investigations. Other information would be needed to reduce the uncertainty in the analysis. This conclusion is also supported based on the wide ranges of Darcy velocities determined herein for the sites considered, in combination with the Project-90 consequence calculations (SKI, 1991).

The analysis shows that at least 10 m of low-percolating rock (*i.e.*, rock with hydraulic conductivity less than or equal to 10^{-10} m/s) is required between the repository and a major percolating zone to guarantee sufficiently low flux through the repository (better than "poor" geosphere performance according to the Project-90 classification, as described in Section 2.1). At some sites at least 100 m of low-percolating rock is required.

The hydraulic characteristics of the disturbed-rock zone (DRZ) have direct implications for groundwater flux through the repository (Winberg, 1991). The DRZ may connect all of the deposition holes with each other, and with previously unconnected conductive elements in the rock intersecting the repository, and may allow significant percolation to occur through the repository. In effect, the DRZ may cause the lack of 10 m or more of low-percolating rock around each canister. On the other hand, it should be noted that, with the detailed discrete-feature model of Äspö (Geier, 1996), inclusion of the DRZ does not markedly affect the predictions. This is partly due to the fact that the fracture network at Äspö is interpreted as already being fairly well-connected, without the DRZ, and partly due to the interpreted, high porosity of the DRZ, which leads to increased residence times for advecting solute.

Thus, although the general effect of the DRZ is to enhance connectivity and percolation through the repository, its influence on performance may be small if the rock already contains a substantial number of high-advective-velocity pathways, as appears to be the case at Äspö.

6 Conclusions

Implications of results for performance assessment

Based upon the available site-characterization data, the geological-barrier function of the Äspö site cannot be confirmed by a simple analysis of flow and transport. The predicted F-ratio values, on which site performance for isolating radionuclides mainly depends, span a very wide range from 10^8 to 10^{16} s/m. Based on this predicted range and consequence calculations carried out within SITE-94 (SKI, 1996), the far-field performance for this site could range anywhere from very poor to very good. The same conclusion is reached based on the analysis of Darcy velocity, using the criterion for Darcy velocity that was established in Project-90 (SKI, 1991).

Implications for site characterization

This simple evaluation shows that it is difficult, if not impossible, to discriminate among the various studied sites in terms of suitability for high-level nuclear waste disposal, on the basis of predicted ranges of Darcy velocity. The wide range of predicted velocities, for Äspö and the other sites studied, is largely a consequence of (1) the high spatial variability of hydraulic conductivity, and (2) conceptual uncertainty regarding how conductive features connect to form pathways for radionuclide release. In order to improve the resolution of performance assessment and allow meaningful discrimination among candidate sites, the following types of site-characterization information would be needed:

1. Characterization of the connectivity among conductive elements in both rock mass and fracture zones (at both the near-field and far-field scales).
2. Site-specific measurements of the properties controlling advective velocities, surface sorption, and matrix diffusion, for transport paths in both the rock mass and in fracture zones (at both near-field and far-field scales).
3. Measurement of changes in transport properties of the rock mass, due to the excavation damaged zone.

In order to confirm the suitability of a given site in terms of the far-field barrier function, it will likely be necessary to demonstrate the existence of, and ability to locate, large volumes

of rock with low percolation *and* high retardation capacity, *e.g.* volumes where the percolation is not concentrated within a few discrete channels.

Relative value of simple vs. detailed analyses in performance assessment

Comparison between this simple evaluation and more detailed hydrological modelling for SITE-94 shows that the simple evaluation yields predicted uncertainty ranges only moderately broader than those predicted by the detailed models. The simple evaluation moreover provides:

- An essential bounding check on the more complex models.
- A straightforward, inexpensive, comprehensible assessment in which the effects of particular assumptions are very easily traced.
- Identification of dominant sources of uncertainty

The detailed models reduce the breadth of the predicted parameter ranges by a few orders of magnitude, but still do not allow for discrimination between acceptable and unacceptable performance, in absolute terms. However, the detailed models are useful and necessary for:

- Discriminating between the effects of spatial variability and other sources of uncertainty.
- Estimating the reasonableness or probabilities of particular parameter combinations, *i.e.* individual values, correlations, and compatible values of different parameters.
- Testing alternative assumptions regarding how different conductive features are connected in space, and alternative assumptions for pore geometry within particular types of features.
- Hydrological evaluation of alternative repository designs.

The detailed models also facilitate quantification of the impact of various types of uncertainty, and thus provide feedback to the site-characterization process.

However both approaches have drawbacks. The simple evaluation cannot directly deal with spatial variability. Complex models must rely upon assumptions about how spatial variability of rock properties and structure that cannot be verified based on site data.

Potential role of simple evaluations in performance assessment

A simple evaluation of groundwater flow and transport parameters, as presented here, can serve as a highly useful component of a complete performance assessment, for the reasons given above. The usefulness of this approach could best be strengthened through research to reduce the uncertainty regarding interrelationships among parameters affecting radionuclide transport within a given transport path.

This simple evaluation is limited to consideration of the geological barrier function and groundwater flow, and thus does not replace other essential components of a performance assessment, such as identification of scenarios or predictions of chemical conditions in the repository. However, the simple evaluation could readily be extended to the evaluation of hydrogeological conditions arising in certain scenarios, such as glaciation.

A simple evaluation provides most of the basic information that can be obtained concerning the range of geological barrier performance (with regard to retardation of radionuclides) that is possible at a given site. This information can be provided rapidly and at a low cost relative to more detailed, numerical modelling. Detailed models are still necessary for specific purposes such as synthesis of data to provide feedback to the site-characterization process, and testing of alternative repository designs. Detailed models are furthermore useful as research tools. Experiments with detailed models can lead to insights that are needed for effective development of simple models.

The closeness of the parameter ranges produced by the simple evaluation and the more detailed models, as given in Section 5.3, indicates that the correct identification of controlling processes and critical parameters is crucial to the successful application of this method. The set-up of a simple evaluation therefore requires a thorough understanding of site data and processes, which can be derived from laboratory and field experiments, from experience with more detailed models, and from basic physical principles. All of these aspects are thus required to develop confidence in a performance assessment based on simple analysis.

7 Acknowledgements

Participation in this study by the co-authors was sponsored by the Swedish Nuclear Power Inspectorate as part of the SITE-94 Project. The authors wish to thank Prof. Ivars Neretnieks of the Royal Technical Institute in Stockholm, and Prof. Ghislain de Marsily of l'Ecole des Mines de Paris, for their insightful and stimulating reviews of this report.

8 Notation

In the following table of notation, reference is made to the pore geometry models (Models A through F), definitions of which may be found in Appendix A.

Symbol	Definition	Dimensions
a_r	Wetted surface area per unit rock (bulk) volume	L^{-1}
a_{rX}	Wetted surface area per unit rock (bulk) volume for Model X, X = A, B, ... F	L^{-1}
a_w	Wetted surface area per unit water volume	L^{-1}
a_{wX}	Wetted surface area per unit water volume for Model X, X = A, B, ..., F	L^{-1}
b	Fracture aperture for Model A	L
b_1, b_2	Aperture values for stepped fractures in Models D and E	L
b_{lim}	Diffusion limit of aperture for Model D	L
b_X	Fracture aperture for Model X, X = B, C, ... F	L
c	$\rho_w g/12\mu_w \approx 8.2\text{x}10^5\ m^{-1}s^{-1}$	$L^{-1}T^{-1}$
C_B	Conductance (product of hydraulic conductivity times cross-sectional area)	L^3/T
dh/dL	Hydraulic head gradient	-
F	F ratio defined as $\frac{a_w L}{\lvert u \rvert} = \frac{a_r L}{\lvert q \rvert}$	T/L
F_X	F ratio for Model X, X = A, B, ... F	T/L
g	Gravitational acceleration $\approx 9.81\ m/s^2$	L/T^2
h	Hydraulic head	L
H	Spacing between transmissive structures	L
K	Hydraulic conductivity	L/T
K_f	Hydraulic conductivity of fracture filling in Model F	L/T
L	Length	L
l	Step spacing in Model E	L
l_1	Offset distance in Model E	L

Symbol	Definition	Dimensions
n	Number of fractures in Model C	-
Q	Flowrate per unit width of transmissive structure	L^2/T
Q'	Volumetric flowrate	L^3/T
q	Darcy velocity (flux)	L/T
q_X	Darcy velocity (flux) for Model X, X = A, B, ... F	L/T
r	Radius	L
r_B	Channel radius in Model B	L
r_f	Grain radius in Model F	L
T	Transmissivity	L^2/T
T_A	Transmissivity of Model A	L^2/T
u	Advective (pore fluid) velocity	L/T
u_X	Advective (pore fluid) velocity for Model X, X = A, B, ... F	L/T
w	Channel (or step) spacing in Model B or D	L
w_1	Offset distance in Model D	L
β	Ratio b_1 / b_2 for Model D or E	L
δ	Matrix thickness	L
θ	Porosity	-
λ	Ratio l_1 / l for Model D	L
μ_w	Viscosity of water $\approx 1.0 \times 10^{-3}$ kg/m·s	M/LT
ρ_w	Density of water ≈ 1000 kg/m^3	M/L^3
ϕ	Porosity of granular fracture filling in Model E	-
ω	Ratio w_1 / w for Model D	L

9 References

Abelin, H., Birgersson, J., Gidlund, J., Moreno, L., Neretnieks, I., Widén, H., and Ågren, T., 3-D Migration experiment – Report 3, Part I. Performed experiments, results and evaluations. Stripa Project Technical Report 87-21, Swedish Nuclear Fuel and Waste Management Co., Stockholm, 1987.

Abelin, H., Birgersson, L., Widén, Ågren, T. , Moreno, L., and Neretnieks, I., Channeling experiment, Stripa Project Technical Report 90-13, Swedish Nuclear Fuel and Waste Management Co., Stockholm, 1990.

Ahlbom, K., Andersson, J-E., Ljunggren, C., Nordqvist, R., Tirén, S., and Voss, C., 1991. Fjällveden study site. Scope of activities and main results. SKB Technical report 91-52, Swedish Nuclear Fuel and Waste Management Co., Stockholm, 1991a.

Ahlbom, K., Andersson, J-E., Ljunggren, C., Nordqvist, R., Tirén, S., and Voss, C., 1991. Gideå study site. Scope of activities and main results. SKB Technical report 91-51, Swedish Nuclear Fuel and Waste Management Co., Stockholm, 1991b.

Ahlbom, K., Andersson, J-E., Andersson, P., Ittner, T., Ljunggren, C., and Tirén, S., 1992. Kamlunge study site. Scope of activities and main results. SKB Technical report 92-15, Swedish Nuclear Fuel and Waste Management Co., Stockholm, 1992a.

Ahlbom, K., Andersson, J-E., Andersson, P., Ittner, T., Ljunggren, C., and Tirén, S., 1992. Klipperås study site. Scope of activities and main results. SKB Technical report 92-22, Swedish Nuclear Fuel and Waste Management Co., Stockholm, 1992b.

Ahlbom, K., Andersson, J-E., Ljunggren, C., Nordqvist, R., Tirén, S., and Voss, C., 1992. Sternö study site. Scope of activities and main results. SKB Technical report 92-02, Swedish Nuclear Fuel and Waste Management Co., Stockholm, 1992c.

Andersson, J-E., Nordqvist, R., Nyberg, G., Smellie, J., and Tirén, S., 1991. Hydrogeological conditions in the Finnsjön area. Compilation of data and conceptual model. SKB Technical Report 91-24, Swedish Nuclear Fuel and Waste Management Co., Stockholm, 1991.

Bear, J., *Dynamics of Fluids in Porous Media.* American Elsevier, New York, 1972.

Dverstorp, B., Andersson, J., and Nordqvist, W., Discrete fracture network interpretation of field tracer migration in sparsely fractured rock, *Water Resources Research*, Vol. 28, No. 9, pp. 2327-2343, 1992.

Geier, J.E., Axelsson, C-L., Hässler, L., and Benabderrahmane, A., Discrete fracture modelling of the Finnsjön rock mass: Phase 2, SKB Technical Report 92-07, Swedish Nuclear Fuel and Waste Management Co., Stockholm, 1992.

Geier, J.E., Doe, T.W., Benabderrahman A., and Hässler, L., Generalized radial flow interpretation of well tests for the SITE-94 project, SKI Report 96:4, Swedish Nuclear Power Inspectorate, Stockholm, 1996.

Geier, J.E., Discrete-feature modelling of the Äspö site: 3. Predictions of hydrogeological parameters for performance assessment (SITE-94), SKI Report 96:7, Swedish Nuclear Power Inspectorate, Stockholm, 1996.

Gentzschein, B., Hydrogeological investigations at the Klipperås study site. SKB Technical Report 86-08, Swedish Nuclear Fuel and Waste Management Co., Stockholm, 1986.

Gustafson, G., Liedholm, M., Lindbom, B., and Lundblad, K. Groundwater flow calculations on a regional scale at the Swedish Hard Rock Laboratory. SKB Progress Report 25-88-17, Swedish Nuclear Fuel and Waste Management Co., Stockholm, 1989.

Gustafson, G., Liedholm, M., Rhén, I., Stanfors, R., and Wikberg, P., Äspö Hard Rock Laboratory. Predictions prior to excavation and the process of their validation. SKB Technical Report 91-23, Swedish Nuclear Fuel and Waste Management Co., Stockholm, 1991.

Gustafsson, E., and Nordqvist, R., Radially converging tracer test in a low-angle fracture zone at the Finnsjön site, central Sweden. The Fracture Zone Project – Phase 3. SKB Technical Report 93-25, Swedish Nuclear Fuel and Waste Management Co., Stockholm, 1993.

KBS, Final storage of spent nuclear fuel – KBS-3. SKBF/KBS Technical Report, Swedish Nuclear Fuel and Waste Management Co., Stockholm, 1983.

Lindbom, B., Lundblad, K., and Winberg, A., Groundwater flow modelling at the Klipperås study site: Regional and subregional scale, SKB Arbetsrapport 88-12, Swedish Nuclear Fuel and Waste Management Co., Stockholm, 1988.

Marone, C. and Scholz, C.H., Particle-size distribution and microstructures within simulated fault gouge, *Journal of Structural Geology*, Vol. 11, pp. 799-814, 1989.

Moreno, L., Gylling, B., and Neretnieks, I., Solute transport in fractured media – The important mechanisms for performance assessment. SKB Technical Report 95-11, Swedish Nuclear Fuel and Waste Management Co., Stockholm, 1995.

Moreno, L., and Neretnieks, I., Fluid and solute transport in a network of channels. SKB Technical report 91-44, Swedish Nuclear Fuel and Waste Management Co., Stockholm, 1991.

Neretnieks, I., Transport in fractured rock. Proceedings of the IAH 17th International Congress on the Hydrology of Rocks of Low Permeability, Tucson, Arizona, January 1985.

Nordqvist, W., Dverstorp, B., and Andersson, J., On the specific surface area parameter: a sensitivity study with a Discrete Fracture network model (SITE-94), SKI Report 95:30, Swedish Nuclear Power Inspectorate, Stockholm, 1995.

Palmqvist, K. and Lindström, M., Channel widths. SKB Technical Report 91-14, Swedish Nuclear Fuel and Waste Management Co., Stockholm, 1991.

Provost, A., Voss, C., and Neuzil, C., Glaciation and regional ground-water flow in the Fennoscandian shield (SITE-94), SKI Report 96:11, Swedish Nuclear Power Inspectorate, Stockholm, 1996.

Rasmuson, A., and Neretnieks, I., Radionuclide transport in fast channels in crystalline rock, *Water Resources Research*, Vol. 22, pp. 1247-1256, 1986.

SKB, SKB 91: Final disposal of spent nuclear fuel. Importance of the bedrock for safety. SKB Technical Report 92-20, Swedish Nuclear Fuel and Waste Management Co., Stockholm, 1992.

SKI SITE-94, Deep repository performance assessment project, SKI Report 96:36, Swedish Nuclear Power Inspectorate, Stockholm, 1996.

SKI, 1991. SKI Project-90. SKI Technical Report 91:23, Swedish Nuclear Power Inspectorate, Stockholm.

Stanfors, R., Erlström, M., and Markström, I., Äspö Hard Rock Laboratory. Overview of the investigations 1986-1990. SKB Technical Report 91-20, Swedish Nuclear Fuel and Waste Management Co., Stockholm, 1991.

Tirén, S., Beckholmen, M., Voss, C., and Askling, P., Development of a geological and structural model of Äspö, southeastern Sweden (SITE-94), SKI Report 96:16, Swedish Nuclear Power Inspectorate, Stockholm, 1996.

Tsang, Y.W., Stochastic Continuum hydrological model of Äspö (SITE-94), SKI Report 96:9, Swedish Nuclear Power Inspectorate, Stockholm, 1996.

Voss, C., and Andersson, J., Regional flow in the Baltic shield during Holocene coastal regression, *Groundwater,* Vol. 31, No. 6, pp. 989-1006, 1993.

Voss, C., Tirén, S., and Glynn, P., Hydrogeology of Äspö Island, Simpevarp, Sweden (SITE-94), SKI Report 96:13, Swedish Nuclear Power Inspectorate, Stockholm, 1996.

Wikberg, P. (ed.), Gustafson, G., Rhén, I., and Stanfors, R., Äspö Hard Rock Laboratory. Evaluation and conceptual modelling based on the pre-investigations 1986-1990. SKB Technical Report 91-22, Swedish Nuclear Fuel and Waste Management Co., Stockholm, 1991.

Winberg, A., The role of the disturbed rock zone in radioactive waste repository safety and performance assessment. A topical discussion and international overview. SKB Technical Report 91-25, Swedish Nuclear Fuel and Waste Management Co., Stockholm, 1991.

Worgan, K., and Robinson, P., The CRYSTAL geosphere transport model: Technical documentation, version 2.1 (SITE-94), SKI Report 95:55, Swedish Nuclear Power Inspectorate, Stockholm, 1995.

Appendix A:

Transport Parameters for Simple Models

In the present analysis, the following simple models are used to account for a wide variety of pore geometries:

A. Simple planar fracture.

B. Simple tubular channels.

C. Multiple planar fractures.

D. Stepped fracture flowing "with the grain," in which the aperture is constant along stream lines, and varies between two values, b_1 and b_2, in the transverse direction.

E Stepped fracture flowing "across the grain," in which the aperture varies between two values, b_1 and b_2, along stream lines.

F Crushed zone modelled as a planar fracture filled with well-packed, spherical grains of uniform radius.

These models are developed in the following sections.

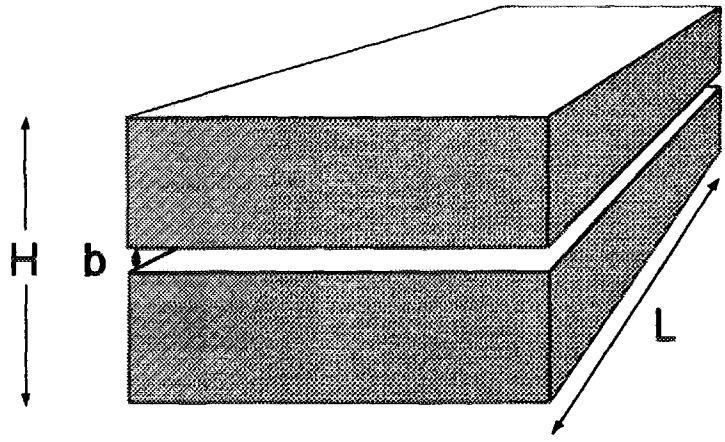

DWG0090I

A.1 Simple planar fracture

For a simple planar fracture with parallel faces (Model A), and conditions of viscous, laminar, steady flow, the relationship between flowrate per unit width Q and hydraulic head gradient dh/dL is:

$$Q = -\frac{\rho_w g b^3}{12 \mu_w} \frac{dh}{dL} = -c b^3 \frac{dh}{dL}$$

where:

b = fracture aperture [m]

ρ_w = density of water $\approx$ 1000 kg/m^3

g = gravitational acceleration $\approx$ 9.81 m/s^2

μ_w = viscosity of water $\approx$ 1.0x10^{-3} kg/m·s at 20° C

c = $\rho_w g/12\mu_w \approx$ 8.2x10^5 m^{-1}s^{-1} at 20° C

The above relationship is often referred to as the "cubic law," because flow is proportional

to the cube of fracture aperture. The transmissivity of the fracture is:

$$T_A = \frac{Q}{dh/dL} = cb^3$$

The mean fluid velocity in the fracture (averaged over the aperture) is:

$$u_A = \frac{Q}{b} = -cb^2\frac{dh}{dL}$$

The wetted surface per unit volume of water is simply:

$$a_{w_A} = \frac{2}{b}$$

The F-ratio for the fracture may be calculated as:

$$F_A = \frac{a_{w_A}L}{|u_A|} = \frac{(2/b)L}{cb^2 dh/dL} = \frac{2L^2}{cb^3\Delta h}$$

for a uniform gradient $dh/dL = \Delta h/L$.

Equivalent porous-medium properties for a fracture, embedded in an effectively impermeable matrix, are dependent upon the essentially arbitrary choice of what thickness of matrix δ to associate with the fracture. Different values of δ may be appropriate depending upon how the parameters are intended to be used.

Here a very simple model for the fractured rock mass is assumed, which consists of a set of parallel, thorough-going fractures with identical aperture and uniform spacing H. For this simple model, the equivalent hydraulic conductivity K for the rock mass is:

$$K = \frac{T_A}{H} = \frac{cb^3}{H}$$

The porosity of this simple model is simply $\theta_A = b/H$, and the wetted surface per unit volume of rock mass is $a_{rA} = 2/H$.

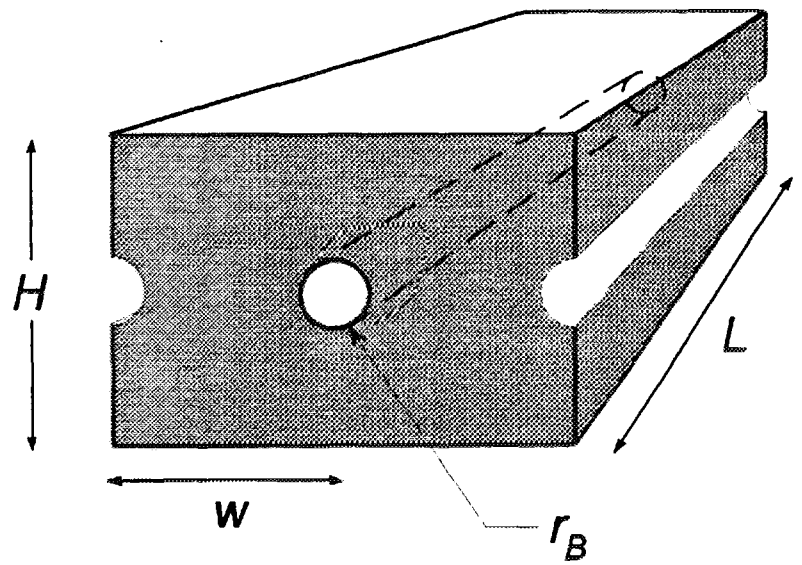

DWG0090J

A.2 Simple tubular channels

For a simple tubular channel, and conditions of viscous, laminar, steady flow, the relationship between volumetric flowrate Q' and hydraulic head gradient is:

$$Q' = -\frac{\pi \rho_w g r_B^4}{8\mu_w}\frac{dh}{dL} = -\frac{3}{2}\pi c r_B^4 \frac{dh}{dL}$$

where r_B is the channel radius. If a planar fracture conducts water via a set of parallel, identical channels, spaced a distance w apart, the equivalent transmissivity of the fracture (in the direction of the channels) is:

$$T = \frac{Q'/w}{dh/dL} = \frac{\frac{3}{2}\pi c r_B^4}{w}$$

The mean fluid velocity (averaged over the cross-sectional area of the channels) is:

$$u_B = \frac{Q'}{\pi r_B^2} = -\frac{3}{2} c r_B^2 \frac{dh}{dL}$$

The wetted surface per unit volume of water is:

$$a_{w_B} = \frac{2\pi r_B}{\pi r_B^2} = \frac{2}{r_B}$$

The F-ratio is, for a uniform gradient $dh/dL = \Delta h/L$:

$$F_B = \frac{a_{w_B} L}{|u_B|} = \frac{(2/r_B) L}{\frac{3}{2} c r_B^2 dh/dL} = \frac{4L^2}{3 c r_B^3 \Delta h}$$

For a channeled fracture with transmissivity equal to that for the simple planar fracture of aperture b, the required radius is:

$$r_B = \left(\frac{2wb^3}{3\pi} \right)^{1/4}$$

As for the simple planar fracture, equivalent porous-medium properties for a channeled fracture, embedded in an effectively impermeable matrix, are dependent upon the arbitrary choice of what matrix thickness δ to associate with the fracture. For identical, channeled fracture planes with a uniform separation H, the equivalent hydraulic conductivity for the rock mass is:

$$K = \frac{T}{H} = \frac{\frac{3}{2}\pi c r_B^4}{wH}$$

The porosity and the wetted surface per unit volume of rock mass are:

$$\theta = \frac{\pi r_B^2}{wH}$$

$$a_{r_B} = \frac{2\pi r_B}{wH}$$

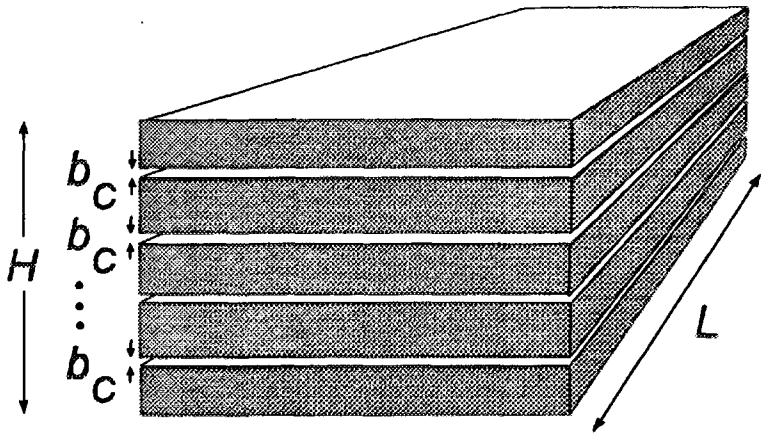

DWG0090K

A.3 Multiple planar fractures

For an idealized fracture zone consisting of n parallel-plate fractures (Model C), each of aperture b_C, the net transmissivity is:

$$T_C = n c b_C^3$$

If T_C is constrained to equal T_A, then the apertures b_C are equal to:

$$b_C = n^{-1/3} b$$

The mean fluid velocity in the fractures is:

$$u_C = -n^{-2/3} c b^2 \frac{dh}{dL} = n^{-2/3} u_A$$

The wetted surface per unit volume of water is:

$$a_{w_C} = \frac{2 n^{1/3}}{b} = n^{1/3} a_{w_A}$$

The F-ratio for a uniform gradient $dh/dL = \Delta h/L$ is:

$$F_C = \frac{a_{w_C} L}{|u_C|} = \frac{2L^2}{c b_C^3 \Delta h} = nF_A$$

For the simple model with an effective fracture-zone or rock-mass thickness equal to H, the equivalent hydraulic conductivity K for the rock mass is:

$$K = \frac{T}{H} = \frac{n c b_C^3}{H}$$

The porosity is $\theta = n^{2/3} b/H$, and the wetted surface per unit volume of rock mass is $a_r = 2n/H$.

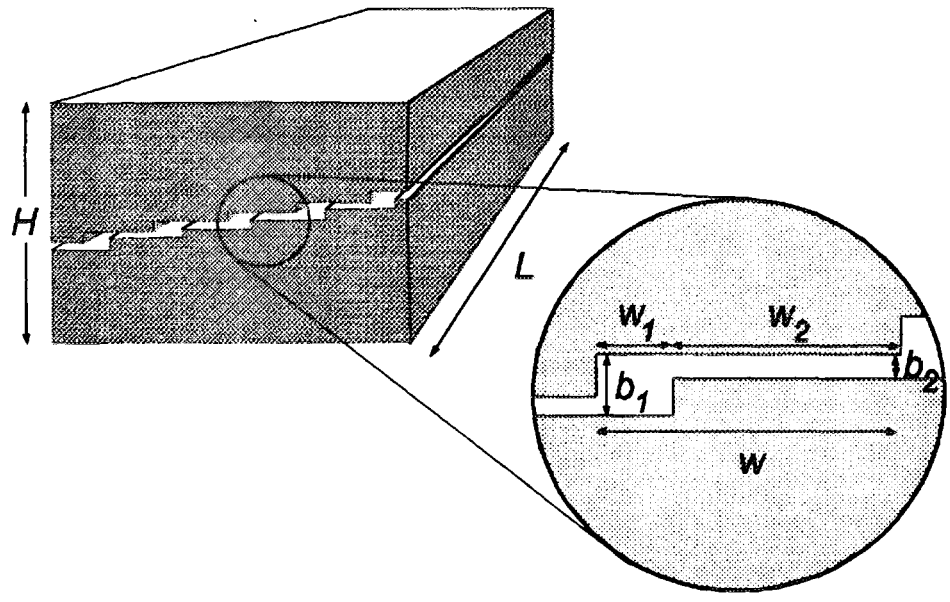

DWG00901

A.4 Model D: Stepped fracture flowing with the grain

For an idealized, uniformly stepped fracture with the direction of flow parallel to the length of the steps (Model D), in which the aperture varies regularly between two values, b_1 and b_2, the net transmissivity in the direction of flow may be calculated approximately by treating each uniform-aperture segment of the fracture as a conductor in parallel, as follows:

Denote the uniform spacing between steps as w, and the offset perpendicular to the steps as w_1, with the constraint $0 < w_1 < w$, based on geometrical considerations, and let $w_2 = w - w_1$. The aperture prior to offset is b_2, and the offset results in an increased aperture $b_1 > b_2$ in the w_1 -wide gap created by the offset.

For a given, uniform gradient dh/dL, the volumetric flowrate through each w_i x b_i segment, where i = 1 or 2, is:

$$Q_i' = -w_i c b_i^3 \frac{dh}{dL}$$

making use of the assumption that each segment can be approximated by a distinct, parallel-plate conduit (thus ignoring any edge effects that may occur near each step). The net flowrate for each step of width w_D is:

$$Q' = Q_1' + Q_2' = -(w_1 b_1^3 + w_2 b_2^3) c \frac{dh}{dL}$$

and the mean Darcy flux (averaged over w_D) is:

$$Q = -(\omega \beta^3 + 1 - \omega) b_D^3 c \frac{dh}{dL}$$

where $\omega = w_1 / w_D$, $\beta = b_1 / b_2$, and $b_D = b_2$. The net transmissivity in the flow direction is thus:

$$T = (\omega \beta^3 + 1 - \omega) c b_D^3$$

If T is constrained to equal T_A, then the aperture b_D is equal to:

$$b_D = (\omega \beta^3 + 1 - \omega)^{-1/3} b$$

The mean fluid velocity in the fracture is:

$$u_D = \frac{Q'}{b_1 w_1 + b_2 w_2}$$

$$= -\frac{\omega \beta^3 + 1 - \omega}{\omega \beta + 1 - \omega} b_D^2 c \frac{dh}{dL}$$

$$= \frac{(\omega \beta^3 + 1 - \omega)^{1/3}}{\omega \beta + 1 - \omega} u_A$$

The wetted surface per unit volume of water is:

$$a_{w_D} = \frac{2(w + b_1 - b_2)}{b_1 w_1 + b_2 w_2}$$

$$= \frac{2(w/b_D + \beta - 1)}{\omega\beta + 1 - \omega}$$

$$= \frac{(\omega\beta^3 + 1 - \omega)^{1/3} + (\beta - 1)\frac{b}{w}}{\omega\beta + 1 - \omega} a_{w_A}$$

The F-ratio for a uniform gradient $dh/dL = \Delta h/L$ is:

$$F_D = \frac{a_{w_D} L}{|u_D|} = \left[1 + \frac{(\beta - 1)\frac{b}{w}}{(\omega\beta^3 + 1 - \omega)^{1/3}}\right] F_A$$

For the simple model with an effective fracture-zone or rock-mass thickness equal to H, the equivalent hydraulic conductivity K for the rock mass is:

$$K = \frac{T}{H} = (\omega\beta^3 + 1 - \omega)\frac{c b_D^3}{H}$$

The porosity of this model is:

$$\theta = \frac{b_1 w_1 + b_2 w_2}{w H}$$

$$= (\omega\beta + 1 - \omega)\frac{b_D}{H}$$

$$= \frac{(\omega\beta + 1 - \omega)}{(\omega\beta^3 + 1 - \omega)^{1/3}} \theta_A$$

and the wetted surface per unit volume of rock mass is:

$$a_{r_D} = \frac{2(w + b_1 - b_2)}{wH}$$

$$= \left[1 + (\beta - 1)\frac{b_D}{w}\right]\frac{2}{H}$$

$$= \left[1 + \frac{\beta - 1}{(\omega\beta^3 + 1 - \omega)^{1/3}}\frac{b}{w}\right]a_{r_A}$$

As $\beta = b_1 / b_2$ becomes very large, eventually b_2 becomes less than some value b_{lim} such that advective transport through the w_2 wide by b_2 thick segments of the fracture may be assumed negligible, and the access to these segments is only via diffusion processes, at a rate comparable to ordinary matrix diffusion. For this case:

$$b_1 \approx \omega^{-1/3} b$$

$$u_D \approx \frac{Q'}{b_1 w_1} \approx -b_1^2 c \frac{dh}{dl} \approx \omega^{-2/3} u_A$$

$$a_{w_D} \approx \frac{2(w_1 + b_1)}{b_1 w_1} \approx \left(\omega^{1/3} + \frac{1}{\omega}\frac{b}{w}\right) a_{w_A}$$

$$F_D \approx \left(\omega + \omega^{-1/3}\frac{b}{w}\right) F_A$$

$$\theta \approx \frac{b_1 w_1}{wH} \approx \omega^{2/3}\theta_A$$

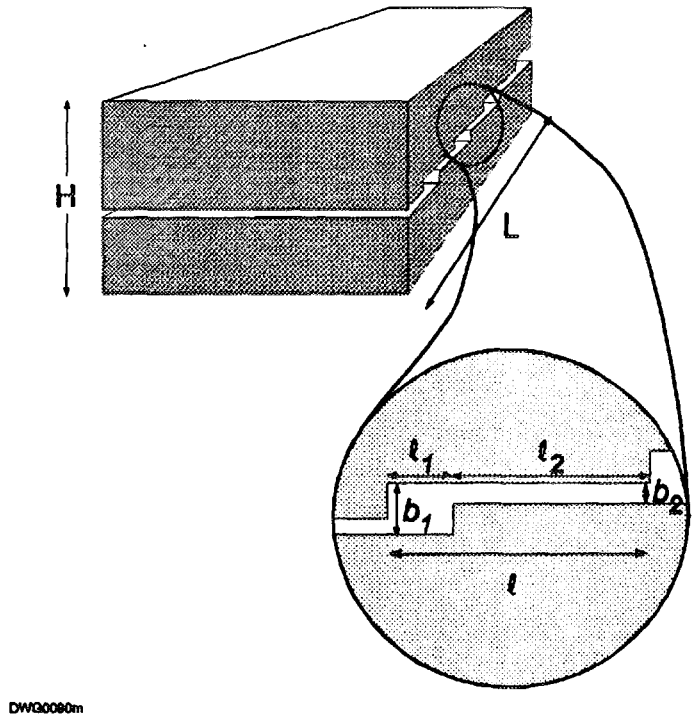

DWG0090m

A.5 Model E: Stepped fracture flowing across the grain

For an idealized, uniformly stepped fracture with the direction of flow perpendicular to the length of the steps (Model E), in which the aperture varies regularly between two values, b_1 and b_2, the net transmissivity in the direction of flow may be calculated approximately by treating each uniform-aperture segment of the fracture as a conductor in series, as follows:

Denote the uniform spacing between steps as l, and the offset perpendicular to the steps as l_1, with the constraint $0 < l_1 < l$, based on geometrical considerations, and let $l_2 = l - l_1$. The aperture prior to offset is b_2, and the offset results in an increased aperture $b_1 > b_2$ in the l_1 -wide gap created by the offset.

For a fixed Darcy flux Q across each segment (conservation of mass under steady flow), the head difference across each l_i long by b_i thick segment, where i = 1 or 2, is:

$$\Delta_i h = -\frac{l_i Q}{c b_i^3}$$

making use of the assumption that each segment can be approximated by a distinct, parallel-plate conduit (thus ignoring any edge effects that may occur near each step). The net head difference over each step of length l is:

$$\Delta_l h = \Delta_1 h + \Delta_2 h = -\left(\frac{l_1}{c b_1^3} + \frac{l_2}{c b_2^3} \right) Q$$

$$= -\left(\frac{\lambda}{\beta^3} + 1 - \lambda \right) \frac{l}{b_E^3} \frac{Q}{c}$$

where $b_E = b_2$, $\lambda = l_1/l$ and $\beta = b_1/b_2$. Thus for a given, average gradient dh/dL, the Darcy flux is:

$$Q = -\left(\frac{\lambda}{\beta^3} + 1 - \lambda \right)^{-1} c b_E^3 \frac{dh}{dL}$$

The net transmissivity in the flow direction is thus:

$$T = \left(\frac{\lambda}{\beta^3} + 1 - \lambda \right)^{-1} c b_E^3$$

If T is constrained to equal T_A, then the aperture b_E is equal to:

$$b_E = \left(\frac{\lambda}{\beta^3} + 1 - \lambda \right)^{1/3} b$$

The mean fluid velocity (averaged over l) in the fracture is:

$$u_E = \frac{l}{\Delta_1 t + \Delta_2 t} = \frac{l}{l_1 b_1/Q + l_2 b_2/Q} = \frac{Q}{\lambda\beta + 1 - \lambda}$$

$$= \frac{-b_E^2 c}{(\lambda/\beta^3 + 1 - \lambda)(\lambda\beta + 1 - \lambda)} \frac{dh}{dl}$$

$$= \frac{(\lambda/\beta^3 + 1 - \lambda)^{-1/3}}{\lambda\beta + 1 - \lambda} u_A$$

The wetted surface per unit volume of water is:

$$a_{w_E} = \frac{2(l + b_1 - b_2)}{b_1 l_1 + b_2 l_2} = \left(\frac{1 + (\beta - 1)\frac{b_E}{l}}{\lambda\beta + 1 - \lambda} \right) \frac{2}{b_E}$$

$$= \frac{(\lambda/\beta^3 + 1 - \lambda)^{-1/3} + (\beta - 1)\frac{b}{l}}{\lambda\beta + 1 - \lambda} a_{w_A}$$

The F-ratio for a uniform gradient $dh/dL = \Delta h/L$ is:

$$F_E = \frac{a_{w_E} L}{|u_E|} = \left[1 + (\beta - 1)(\lambda/\beta^3 + 1 - \lambda)^{1/3} \frac{b}{l} \right] F_A$$

For the simple model with an effective fracture-zone or rock-mass thickness equal to H, the equivalent hydraulic conductivity K for the rock mass is:

$$K = \frac{T}{H} = (\lambda/\beta^3 + 1 - \lambda)^{-1} \frac{c b_E^3}{H}$$

The porosity of this model is:

$$\theta = \frac{b_1 l_1 + b_2 l_2}{lH}$$

$$= (\lambda\beta + 1 - \lambda)\frac{b_E}{H}$$

$$= (\lambda\beta + 1 - \lambda)(\lambda/\beta^3 + 1 - \lambda)^{1/3}\theta_A$$

and the wetted surface per unit volume of rock mass is:

$$a_{r_E} = \frac{2(l + b_1 - b_2)}{lH} = \left[\lambda + (\beta - 1)\frac{b_E}{l}\right]\frac{2}{H}$$

$$= \left[\lambda + (\beta - 1)(\lambda/\beta^3 + 1 - \lambda)^{1/3}\frac{b}{l}\right]a_{r_A}$$

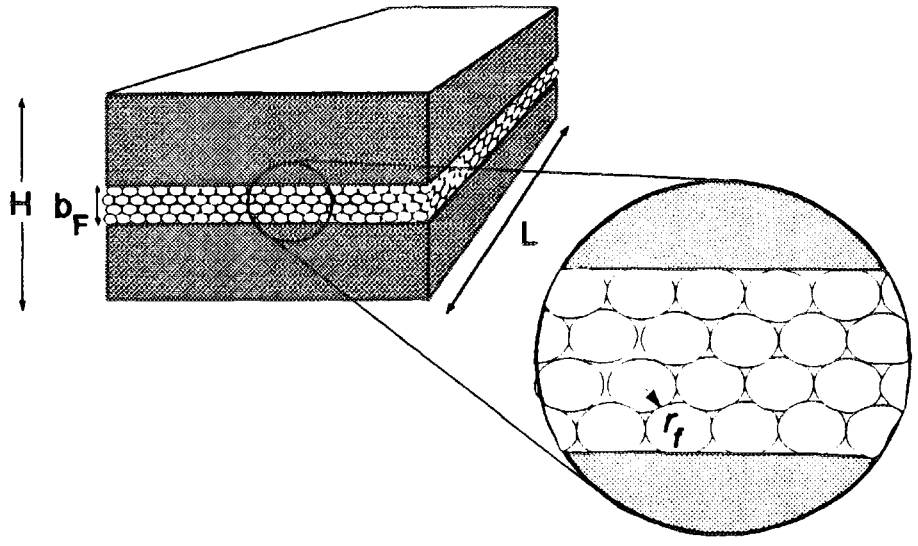

DWG0080n

A.6 Model F: Crushed zone

For a parallel-plate fracture of aperture b_F, filled with spherical grains of uniform radius r_f, the transmissivity can be calculated as follows.

The permeability of the fracture filling (*i.e.*, the packed spherical grains) is, according to the Carman-Kozeny equation (see Bear, 1972):

$$k_f = \frac{\phi^3}{(1-\phi)^2}\frac{r_f^2}{45}$$

where ϕ is the porosity of the packed spheres, which depends upon the type of packing (*e.g.* for hexagonal packing, $\phi = 1 - \pi/3\sqrt{2}$).

The hydraulic conductivity of the fracture filling is:

$$K_f = \frac{k_f \rho_w g}{\mu_w} = \frac{4}{15}\frac{\phi^3 r_f^2 c}{(1-\phi)^2}$$

from which the transmissivity of the sphere-filled fracture is obtained directly as:

$$T = \frac{4}{15}\frac{\phi^3 r_f^2}{(1-\phi)^2} c\, b_F$$

If T is constrained to equal T_A, then the sphere radius r_f is equal to:

$$r_f = \frac{(1-\phi)b}{2\phi}\left(\frac{15}{\phi}\frac{b}{b_F}\right)^{1/2}$$

The mean fluid velocity in the fractures is:

$$u_F = \frac{-K_f b_F}{\phi b_F}\frac{dh}{dL} = -\frac{4}{15}\frac{\phi^2 r_f^2 c}{(1-\phi)^2}\frac{dh}{dL} = \left(\frac{b}{\phi b_F}\right) u_A$$

The wetted surface per unit volume of water is:

$$a_{w_F} = \frac{3}{r_f \phi} = \sqrt{\frac{3}{5}}\frac{1}{(1-\phi)}\sqrt{\frac{\phi b_F}{b}}\, a_{w_A}$$

The F-ratio for a uniform gradient $dh/dL = \Delta h/L$ is:

$$F_F = \frac{a_{w_F} L}{|u_{FC}|} = \frac{45}{4}\frac{(1-\phi)^2 L^2}{\phi^3 r_f^3 c\, \Delta h} = \sqrt{\frac{3}{5}}\frac{1}{(1-\phi)}\left(\frac{\phi b_F}{b}\right)^{3/2} F_A$$

For the simple model with an effective fracture-zone or rock-mass thickness equal to H, the equivalent hydraulic conductivity for the rock mass is:

$$K = \frac{K_f b_F}{H} = \frac{4\phi^3 r_f^2 c\, b_F}{15(1-\phi)^2 H}$$

The porosity of this simple model is $\theta = \phi b_F/H = (\phi b_F/b)\theta_A$, and the wetted surface per unit volume of rock mass is $a_{rF} = 3b_F/r_f H$.

STATENS KÄRNKRAFTINSPEKTION
Swedish Nuclear Power Inspectorate

Postadress/Postal address	Telefon/Telephone	Telefax	Telex
SKI S-106 58 STOCKHOLM	Nat 08-698 84 00 Int +46 8 698 84 00	Nat 08-661 90 86 Int +46 8 661 90 86	11961 SWEATOM S